Simulation and Analysis of Wind Turbine Loads for Neutrally Stable Inflow Turbulence

by

Chungwook Sim, B.S., M.S.

THESIS

Presented to the Faculty of the Graduate School of
The University of Texas at Austin
in Partial Fulfillment
of the Requirements
for the Degree of

MASTER OF SCIENCE IN ENGINEERING

THE UNIVERSITY OF TEXAS AT AUSTIN
August 2009

Simulation and Analysis of Wind Turbine Loads for Neutrally Stable Inflow Turbulence

APPROVED BY

SUPERVISING COMMITTEE:

Lance Manuel, Supervisor

Loukas F. Kallivokas

Dedicated to my wife Jisun and our family

Acknowledgments

The author would like to express gratitude to his thesis advisor Dr. Lance Manuel for continuous support, encouragement and guidance during this research and graduate studies.

The author appreciates Dr. Loukas F. Kallivokas for reading this thesis and giving thoughtful advice. The author especially thanks Dr. Sukanta Basu at Texas Tech University who gave full assistance for all of the numerical simulation work related to the field of atmospheric science. The author would like to express gratitude to Dr. James O. Jirsa, Dr. John L. Tassoulas, Dr. Michael D. Engelhardt, and Dr. Sharon L. Wood for their expertise on structural engineering, academic guidance, and support that gave inspiration to the author's graduate studies.

This study was financially supported by Sandia National Laboratories (by way of Contract No: 743358) and the Texas Higher Education Coordinating Board's Advanced Research Program (Grant No. 003658-0100-2007). Their support is gratefully acknowledged.

Finally, the author thanks his parents and parents-in-law for their unconditional love and patience. Sincere thanks are extended to Jisun for her warm encouragement, love, and belief in the author.

Simulation and Analysis of Wind Turbine Loads for Neutrally Stable Inflow Turbulence

Chungwook Sim, M.S.E.
The University of Texas at Austin, 2009

Supervisor: Lance Manuel

Efficient temporal resolution and spatial grids are important in simulation of the inflow turbulence for wind turbine loads analyses. There have not been many published studies that address optimal space-time resolution of generated inflow velocity fields in order to estimate accurate load statistics. This study investigates turbine extreme and fatigue load statistics for a utility-scale 5MW wind turbine with a hub-height of 90 m and a rotor diameter of 126 m. Load statistics, spectra, and time-frequency analysis representations are compared for various alternative space and time resolutions employed in inflow turbulence field simulation. Conclusions are drawn regarding adequate resolution in space of the inflow turbulence simulated on the rotor plane prior to extracting turbine load statistics. Similarly, conclusions are drawn with regard to what constitutes adequate temporal filtering to preserve turbine load statistics. This first study employs conventional Fourier-based spectral methods for stochastic simulation of velocity fields for a neutral atmospheric boundary layer.

In the second part of this study, large-eddy simulation (LES) is employed with similar resolutions in space and time as in the earlier Fourier-based simulations to again establish turbine load statistics. A comparison of extreme and fatigue load statistics is presented for the two approaches used for inflow field generation. The use of LES-generated flows (enhanced in deficient high-frequency energy by the use of fractal interpolation) to establish turbine load statistics in this manner is computationally very expensive but the study is justified in order to evaluate the ability of LES to be used as an alternative to more common approaches. LES with fractal interpolation is shown to lead to accurate load statistics when compared with stochastic simulation. A more compelling reason for using LES in turbine load studies is the following: for stable boundary layers, it is not possible to generate realistic inflow velocity fields using stochastic simulation. The present study presents a demonstration that, despite the computational costs involved, LES-generated inflows can be used for loads analyses for utility-scale turbines. The study sets the stage for future computations in the stable boundary layer where low-level jets, large speed and direction shears across the rotor, etc. can possibly cause large turbine loads; then, LES will likely be the inflow turbulence generator of choice.

Table of Contents

List of Tables

List of Figures

Chapter 1

Introduction

1.1 Background

The World Wind Energy Association (WWEA) estimates that the total wind energy installed worldwide will be 152 GW by the end of 2009. This is only 1% of the total energy consumption in the world but it is eight times higher than the wind energy produced in 2000. Even with the current world economic crisis, the increase in wind energy this year will be one-quarter of the total wind energy produced in 2008 (121 GW). In some countries, such as Denmark, Germany, and Spain, the target for wind energy is 10% or more of the total electricity capacity. It is becoming increasingly evident that wind energy is growing at a rapid pace as an alternative energy source.

Along with the rapid growth of wind energy, the industry's technologies are getting more complex and the size of the wind turbines are increasing as well. The hub height of some of today's wind turbines has increased by more than three times compared to wind turbines used in the first commercial wind farms from the 1980s. Their capacity has increased more by almost an order of magnitude than around 500KW to around and upwards of 5,000KW (or 5MW). With such turbines, rotors sweep very large areas and distances (laterally and vertically). As a result, the ability to accurately simulate inflow turbulence is essential in designing today's wind turbine blades and tower.

1.2 Background and Research Motivation

The principal standard that is used in the design of wind turbines has been provided by the International Electrotechnical Commission (IEC) [11]. Det Norske Veritas(DNV) and the RisøNational Laboratory in Denmark have also published standards and guidelines for the design of wind turbines [24]. These documents recommend models to generate the inflow turbulence and suggest procedures to estimate extreme and fatigue loads on wind turbines.

The IEC proposes two turbulence models for design calculations: the Mann uniform shear turbulence model and the Kaimal spectral and exponential coherence model. The DNV guidelines recommend the Harris and Kaimal spectra to be used for stochastic turbulence generation. These turbulence models describe spectral density functions that define distribution of energy in turbulence over all frequencies. The mean longitudinal wind velocity component that varies with elevation is defined by a wind speed shear law; at hub height, its ten-minute average is defined as a random variable with a Rayleigh or Weibull probability distribution. The transverse and vertical wind velocity components have zero means in conventional stochastic simulation for wind turbines. In wind turbine load studies, ten-minute turbulence time series generated using prescribed power spectra and coherence functions describe a zero-mean stationary Gaussian random field representing the three turbulence components (u: longitudinal, v: lateral, and w: vertical) at grid points on the rotor plane [11, 24].

In the IEC guidelines for wind turbine design [11], the recommended "normal turbulence model" assumes that stationary spectral representations can serve as the basis for stochastic simulation of inflow turbulence fields. Only near-neutral stability conditions are considered in such simulations. However, recent studies suggest that significant fatigue damage can occur from coherent structures that are produced in flows common in the stable nocturnal atmospheric boundary layer [16]. Moreover, the non-stationary character of the wind velocity processes, not represented in the IEC turbulence models, can be another important influence on wind turbine loads.

Over the past two decades, there has been considerable wind energy development in the Great Plains regions of the U.S. where nocturnal low-level jets (LLJs) occur quite frequently. The peaks (or identifiable local maxima in the vertical wind profiles) of LLJs are typically centered around 100-1,000 m above the ground level and make the Great Plains' wind resources favorable for wind energy production. At the same time, the presence of these LLJs can significantly modify vertical shear and night-time turbulence environments in the vicinity of wind turbine hub heights; this can have a detrimental effects on rotors [15].

Thus, accurate numerical modeling of such inflow turbulence fields is needed for robust wind turbine design and for more reliable power generation prediction. Since stable stratification is a prerequisite for the occurrence of nocturnal inflow turbulence, this then requires an improved modeling capability of stable boundary layers (SBLs). An example of such modeling using Large-Eddy Simulation (LES) is demonstrated in Fig 1.1.

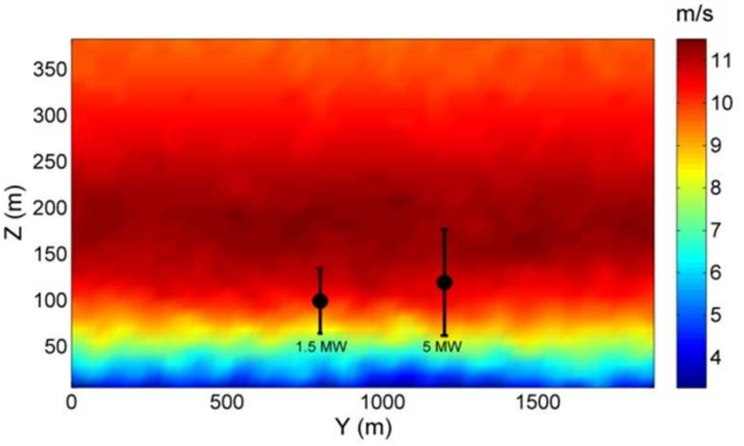

Figure 1.1: Lateral cross-section of the mean longitudinal wind speed field generated for SBL conditions by an LES model.

The hubs and rotor tips of two contemporary wind turbines are depicted in Fig 1.1. The 5MW turbine rotor will experience strong shear over a 60-120 m vertical band (in Fig. 1.1, the lower rotor tip of the 5MW turbine experiences a wind speed of around 8 m/s, whereas the upper tip experiences a wind speed close to 11 m/s). In addition, the dark red bands of higher wind speeds in the 100-250 m range indicated the occurrence of a low-level jet. Sporadic bursts of turbulence (indicated by turbulence kinetic energy) in the midst of otherwise quiescent stable stratified conditions are also clearly visible in Fig 1.2.

Clearly, SBL flow generation is of interest because of the need to understand the influence of such flows on wind turbine loads. While LES may

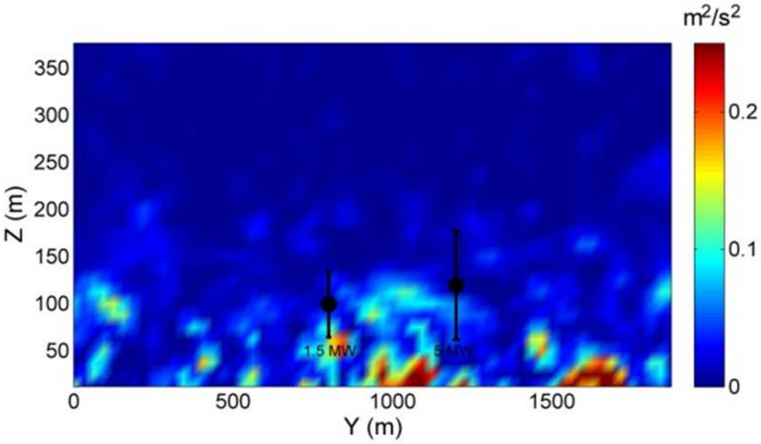

Figure 1.2: Lateral cross-section of the turbulence kinetic energy field generated for SBL conditions by an LES model.

be used to generate such SBL flows, conventional stochastic simulation (using Fourier techniques) is incapable of generating these flows. We are interested ultimately in understanding SBL flows and their effects on wind turbine loads. Logically, we would like to address that question immediately. However, it is of interest to examine how loads from LES and conventional simulation flows differ in situations where both methods can be employed for inflow turbulence simulation. Such a comparison is possible for neutral boundary layers (NBL).

As a preliminary study for future LES applications in addressing wind turbine loads under stable boundary layer inflow, a comparison of turbine loads for neutrally stable boundary layer inflow produced based on LES and conventional stochastic simulations is the focus of this study.

Computational effort involved in LES flow generation is considerably more challenging than is the case for flow generation using conventional stochastic simulation. We are interested in accurate turbine load statistics but we are also interested in efficiency in computational spatial grids and temporal sampling for LES. Because we must make consistent comparisons between flows and turbine loads generated using conventional stochastic simulation and LES, the first part of our study addresses efficiency in temporal and spatial resolution of NBL flows (and resulting loads) using conventional stochastic simulation alone. Next, after we determine the most efficient spatio-temporal inflow representation, we compare loads from LES and conventional simulation approaches using these spatial grids and time steps. We compare various turbine load statistics that relate to wind turbine ultimate and fatigue limit states.

1.3 Research Procedure and Scope

The primary goal of this research is to demonstrate that LES can be applied in wind turbine load studies. As stated previously, SBL flows and associated loads can be generated using LES but not by conventional stochastic simulation procedures in common use. This is the motivation for our work. We will compare the inflow turbulence generated from LES with that from conventional Fourier-based stochastic simulation.

Figure 1.3 shows a flow chart representing various related tasks involved in this research study. Large-eddy simulation (LES) and stochastic simulation will serve as alternative approaches for generating inflow turbulence over the rotor swept area of our 5MW turbine. These inflow fields will serve as inputs for turbine aeroelastic simulation where structural dynamics, aerodynamics, and control systems are modeled. Output time series data on various load measures are analyzed and these then feed into turbine load studies where load statistics are summarized using time-domain methods, frequency-domain methods, and time-frequency analysis using wavelets.

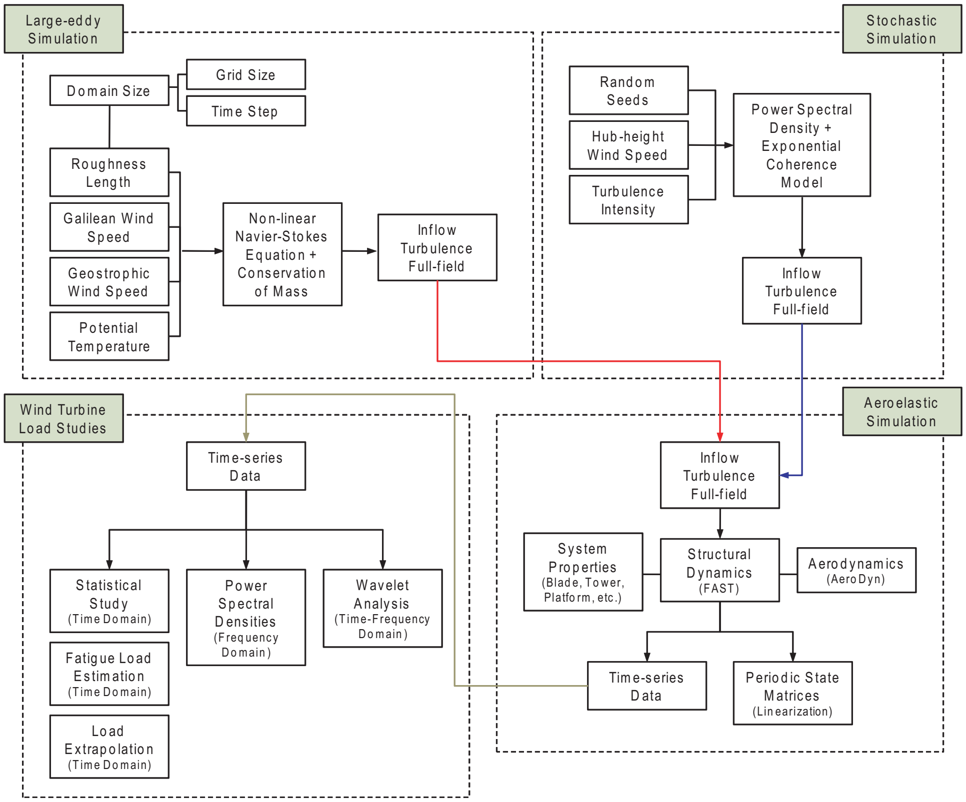

Figure 1.3: Outline of inflow and turbine load simulation and statistical studies.

This research addresses, in order, the following topics: (i) efficiency in spatial and temporal sampling of inflow turbulence based on conventional stochastic simulation; (ii) LES-generated NBL inflow fields and comparison with conventional stochastic simulation; and (iii) load statistics comparisons for the alternative flow fields generated in (ii).

1.4 Thesis Organization

Chapter 2 addresses the question of efficiency of temporal sampling and of spatial computation grids required for numerical simulation of inflow turbulence for large wind turbines. For both inflow turbulence and wind turbine loads, statistical summaries, spectral characteristics, and wavelet analyses will be presented. Conclusions will be reached, based only of these conventional stochastic simulations, on acceptable space and time discretization of inflow fields for turbine load studies.

Inflow turbulence based on LES and stochastic simulation are compared in Chapter 3. Fractal interpolation will be discussed as a means to enhance LES fields with missing high-frequency energy.

Chapter 4 estimates extreme and fatigue loads for NBL inflow turbulence fields generated in Chapter 3. Wind turbine load statistics, time series, and power spectra are studied. Fatigue loads are studied ane extreme load probability distributions are also presented.

A summary of this entire research study is presented Chapter 5 along with some key conclusions and recommendations for future research.

Chapter 2

The Influence of Temporal and Spatial Sampling of Inflow Turbulence on Wind Turbine Loads

2.1 Introduction

Very few studies to date have addressed the question of efficiency of sampling (or resolution) that is adequate when generating inflow velocity files for purposes of estimating accurate load statistics for today's large utility-scale wind turbines. The present study takes on this question by making use of conventional stochastic simulation of stationary Gaussian fields using Fourier methods.

We study here loads on one such utility-scale wind turbine (rated at 5 MW) that has a hub height of 90 meters and a rotor diameter of 126 meters. Our interest is in determining an acceptable frequency resolution for the inflow turbulence generation so that resulting turbine load statistics (extremes and fatigue) can be predicted without loss of accuracy. Spectral filtering of the "base inflow" generated at 32 Hz sampling is applied in the frequency domain to generate samples with some intentional loss of high-frequency energy. Likewise, grid resolution on the rotor plane (which represents a square, 140 m on each side) is varied to different degrees of coarseness and loads studied following aeroelastic simulation. The dynamic characteristics of turbine loads including flapwise bending moment at a blade root, edgewise bending moment at a blade root, fore-aft tower base bending moment, and tower top fore-aft displacement are studied.

We conclude with recommendations for efficient spatio-temporal inflow simulation schemes that lead to turbine extreme and fatigue load statistics that are reasonably accurate for design purposes. These grid and temporal resolutions will later be employed in studies involving the use Large-Eddy Simulation (LES) for load computations.

2.2 Stochastic Simulation Model

The Fourier-based stochastic turbulence simulation code, TurbSim [13], was used to generate the “base inflow” for this study. TurbSim, developed at the National Renewable Energy Laboratory (NREL), is based on SNLWIND, which was in turn developed at Sandia National Laboratories [23]. Such codes are used to stochastically generate full spatio-temporal wind velocity fields. The Kaimal power spectral density (PSD) function was used for the turbulence generation. It can be expressed as follows:

$$\frac{f \cdot S_k(f)}{\sigma_k^2} = \frac{4f \cdot L_k/V_{hub}}{(1 + 6f \cdot L_k/V_{hub})^{5/3}} \tag{2.1}$$

where f represents frequency in Hz; k is an index referring to the direction of the wind velocity component (k is set equal to 1, 2, or 3 for the longitudinal, lateral, and vertical components, respectively); $S_k(f)$ is the single-sided power spectral density function for wind velocity component, k; σ_k is the standard deviation for the wind velocity component k; L_k is the integral scale parameter for wind velocity component, k; and V_{hub} is the ten-minute average hub-height longitudinal wind speed. Values for the three wind velocity component standard deviations and integral scale parameters are specified in the IEC 61400-1 guidelines [11].

An exponential coherence function specified in the IEC 61400-1 guidelines [11] was also used in this study. This function is expressed as follows:

$$Coh(r, f) = \exp\left[-12\left((f \cdot r/V_{hub})^2 + (0.12r/L_c)^2\right)^{0.5}\right] \tag{2.2}$$

where the coherence function, $Coh(r, f)$, is defined as the magnitude of the complex cross-spectral density funciton of the longitudinal wind velocity component at two spatially separated points divided by the autospectrum function; r is the magnitude of the projection of the separation vector between the two points on to a plane normal to the average wind direction; and L_c is the coherence scale parameter.

The "normal turbulence model" with a reference turbulence intensity of 16% (corresponding to Wind Turbine Site Class A) was used to generate the inflow velocity field. Using the normal turbulence model (NTM), the power spectra, coherence functions, and reference turbulence intensity, full wind fields were stochastically generated on a rotor plane for the wind turbine selected. A time step of 0.03125 seconds (representing 32 Hz sampling) was used to generate the "base inflow" turbulence. Table 2.1 summarizes various parameters and their values used in the inflow simulation with TurbSim. These inflow fields for three different wind speeds were filtered in the frequency domain using low-pass filters with cut-off frequencies set at 16 Hz, 8 Hz, 4 Hz, 2 Hz, 1 Hz, 1/2 Hz, 1/4 Hz, and 1/8 Hz.

Table 2.1: Parameters and values used in inflow turbulence field simulation.

Parameters	Values
Hub height (m)	90
Hub-height wind speed (m/s)	12, 15, 18
Base sampling rate (Hz)	32
Low-pass cut-off frequency (Hz)	16, 8, 4, 2, 1, 0.5, 0.25, 0.125
Grid (x × y)	13 × 13, 11 × 11, 9 × 9
Surface roughness (m)	0.1

The rotor plane of the selected 5MW turbine model [14] with a rotor diameter of 126 m is represented in separate analyses by 13×13, 11×11, and 9 ×9 grids that cover a square area of side 140 m, centered at the rotor hub. The 5MW wind turbine model closely represents a utility-scale wind turbine that is currently being manufactured. This model is used for our aeroelastic response simulations. The turbine is a variable-speed, collective pitch-controlled machine. Four different turbine loads are studied; these include the flapwise bending moment at a blade root (FBM), the edgewise bending moment at a blade root (EBM), the tower base fore-aft bending moment (TBM), and the tower top fore-aft displacement (TTD). Ten-minute time series of these loads are simulated using the aeroelastic simulation tool, FAST [12], developed at NREL. The natural frequencies of our turbine model were checked with the

FAST linearization mode to determine possible energetic frequency ranges of response that the turbine might experience. Table 2.2 summarizes information on the natural modes of vibration and their associated frequencies.

Table 2.2: Natural modes of vibration for the wind turbine model.

Natural freq. range (Hz)	Natural mode
0.37 - 0.38	1st tower side-to-side bending mode 1st tower fore-aft bending mode
0.63 - 0.67	1st flapwise bending mode of blades
1.08 - 1.09	1st edgewise bending mode of blades
1.94 - 1.95	2nd flapwise bending mode of blades
3.36-3.38	2nd tower fore-aft bending mode 2nd tower side-to-side bending mode

2.3 Filtering of Inflow Turbulence

To the base inflow (at a 32 Hz sampling rate) obtained from TurbSim, a low-pass filter was applied in the frequency domain with cut-off frequencies defined as given in Table 2.1. Zero padding and filtered time series were obtained without changing the number of samples in the time domain.

Power spectral densities (PSDs) computed for the various filtered longitudinal wind velocity time series at hub height are presented in Fig. 2.1. These estimated PSDs are based on an ensemble of 15 ten-minute simulations in each case. The PSDs are shown only up to 16 Hz, the Nyquist frequency, since all the inflow time series have an identical time step of 0.03125 seconds

(32 Hz). The log-log plot shows that the inflow time series, with or without the filtering, all follow Kolmogorov's -5/3 power law for scaling of turbulence in the inertial subrange. The target Kaimal power spectrum for longitudinal turbulence at hub height is also shown in Fig. 2.1; the simulated PSD for the unfiltered case matches the target spectrum well; it is slightly deficient in power at frequencies above around 8 Hz. As increased filtering is applied, the PSDs drop at lower and lower frequencies as expected.

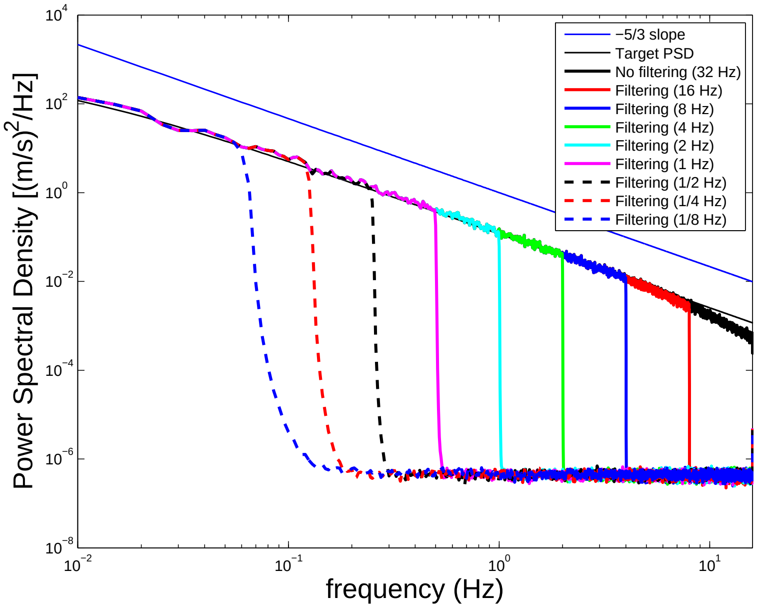

Figure 2.1: Target Kaimal PSD and estimated PSDs from unfiltered and filtered simulated hub-height longitudinal inflow turbulence.

Figures 2.2 to 2.5 show the effect of filtering of the longitudinal wind velocity at hub height as low-pass filters are applied successively at 16 Hz, 4 Hz, 1 Hz, and 1/4 Hz. The top plot in each figure shows, with black lines, the unfiltered (32 Hz) wind velocity time histories generated by TurbSim; the filtered time series are shown with red lines. A zoomed-in portion of the times series between 50 and 80 seconds (in the middle plot of each figure) shows that the general low-frequency trends are preserved; at this display scale, only high-frequency fluctuations are affected by filtering. As the amount of filtering that is applied increases, differences between the unfiltered and filtered time series data increase; this is evident in the bottom plots of each figure.

Figure 2.6 shows the fraction of the unfiltered longitudinal wind velocity variance recovered after various temporal filtering that results at all locations on a 13×13 grid representing the rotor plane for hub-height ten-minute mean wind speeds of 12 m/s, 15 m/s, and 18 m/s. This is summarized in parts (a), (c), and (e) of the figure. Similar plots for 12 m/s, 15 m/s, and 18 m/s are presented in parts (b), (d), and (f) of the figure based on simulations on a 9×9 grid.

Note that the fraction of variance retained after filtering at any location on the rotor plane is farther from the target (unfiltered) case as the filtering is increased. The overall trends are not very different for the two spatial grid and for the three wind speeds. More importantly, it may be seen that the variance (or energy) in the turbulence field is reasonably accurate (with less than 5% error) at all locations on the rotor plane if filtering is allowed only above 1 Hz. Stated differently, with a 1 Hz filter, turbulence variance is within 5% of the unfiltered level at all locations, for all three wind speeds, and with both spatial grids.

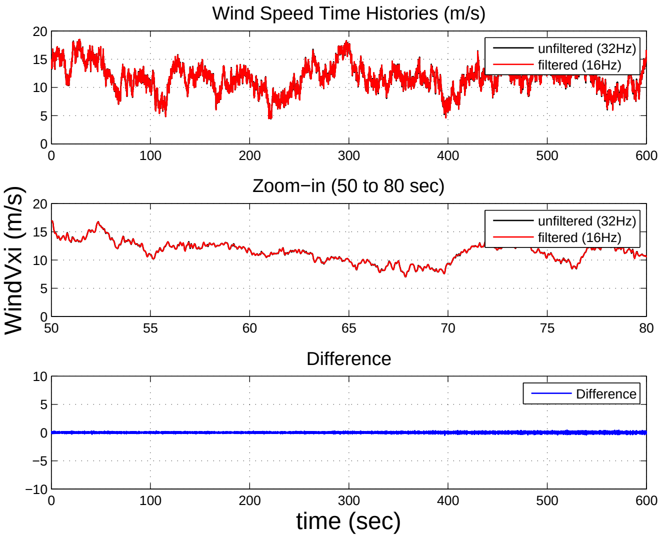

Figure 2.2: Inflow turbulence time histories with 16 Hz filter.

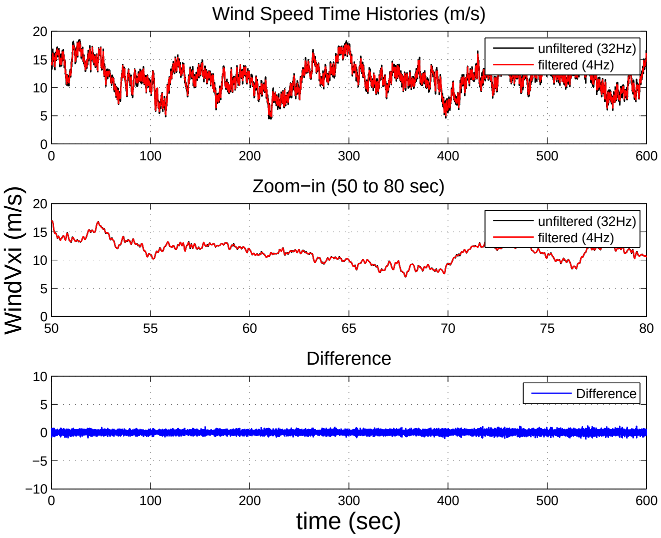

Figure 2.3: Inflow turbulence time histories with 4 Hz filter.

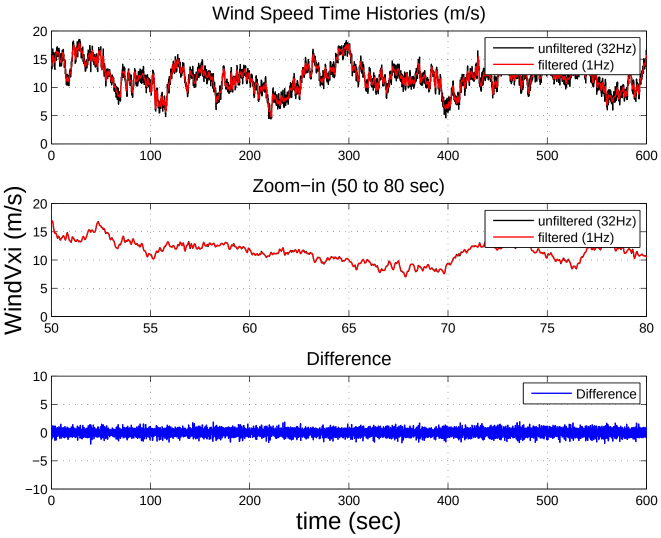

Figure 2.4: Inflow turbulence time histories with 1 Hz filter.

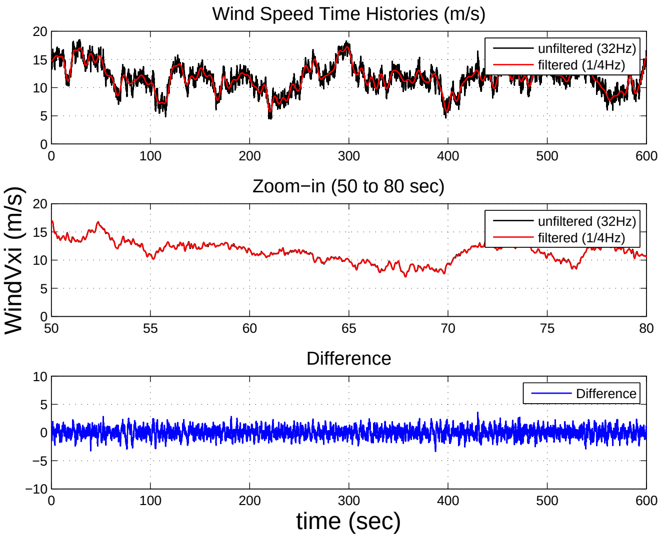

Figure 2.5: Inflow turbulence time histories with 0.25 Hz filter.

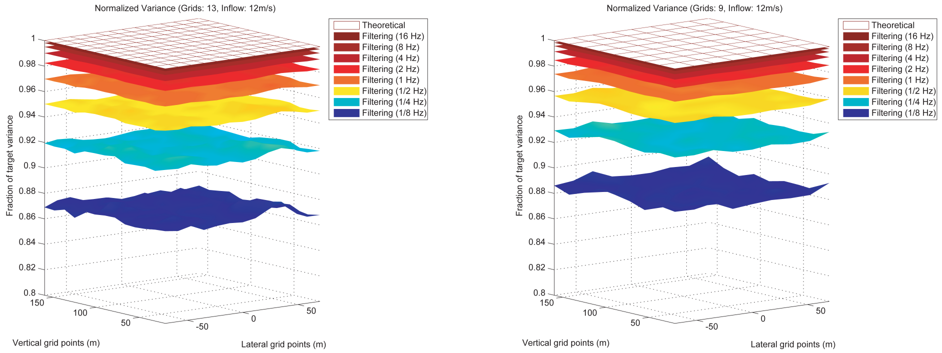

(a) 13×13; 12 m/s (b) 9×9; 12 m/s

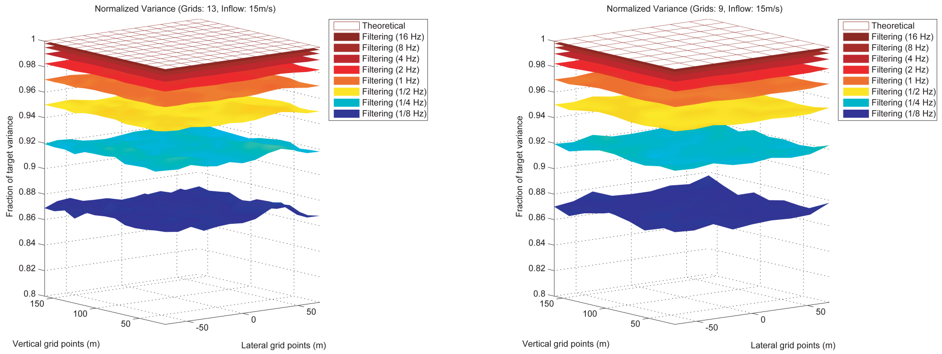

(c) 13×13; 15 m/s (d) 9×9; 12 m/s

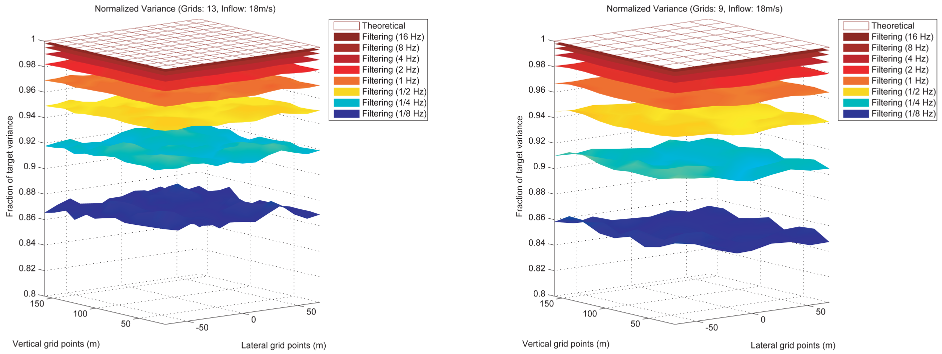

(e) 13×13; 18 m/s (f) 9×9; 18 m/s

Figure 2.6: Fraction of the unfiltered longitudinal wind velocity variance recovered after various temporal filterings on a 13×13 grid for hub-height mean wind speeds of (a) 12 m/s, (c) 15 m/s, and (e) 18 m/s; and on 9×9 grid for hub-height mean wind speeds of (b) 12 m/s, (d) 15 m/s, and (f) 18 m/s.

2.4 Turbine Load Statistics

2.4.1 Spatial sampling of inflow turbulence

We are interested in turbine load statistics for the various inflow time series generated. These inflow velocity time series are generated for (i) three different hub-height mean wind speeds (12 m/s, 15 m/s, and 18 m/s); (ii) three different spatial grids/samplings on the rotor plane (13×13, 11×11, and 9×9); and (iii) eight different filters (low-pass filters applied at 16 Hz, 8 Hz, 4 Hz, 2 Hz, 1 Hz, 1/2 Hz, 1/4 Hz, and 1/8 Hz). We estimate the standard deviation, the ten-minute extreme, and the equivalent fatigue load (EFL) for four different turbine loads (FBM, EBM, TBM, and TTD). A total of fifteen simulations were used to summarize ensemble load statistics for each load for the various inflow time series. Note that for the EFL calculations, a Wohler exponent of 10 was applied for FBM and EBM; for TBM and TTD, a Wohler exponent of 3 was used.

First, we address the matter of spatial and temporal sampling of the inflow turbulence and its influence on load statistics. Figures 2.7 to 2.10 show bar charts of turbine blade and tower load statistics for three different hub-height wind speeds and four different spatial arrays including an additional 9×9 grid with a 1 Hz-filtered inflow.

Ensemble standard deviation estimates of the four loads studied show very slight variation with hub-height mean wind speed. Only the FBM standard deviation shows a slight increasing trend with wind speed. The various spatial grids and even the 9×9 grid with a 1 Hz filter do not lead to large

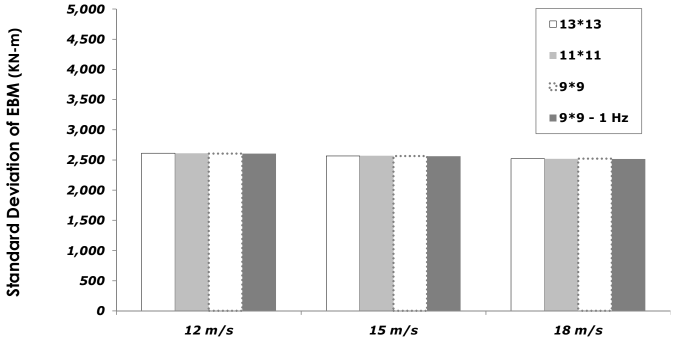

(a) Standard Deviation of EBM

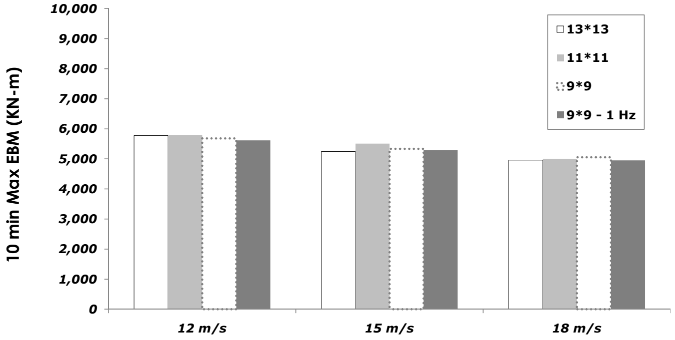

(b) 10-min Extreme of EBM

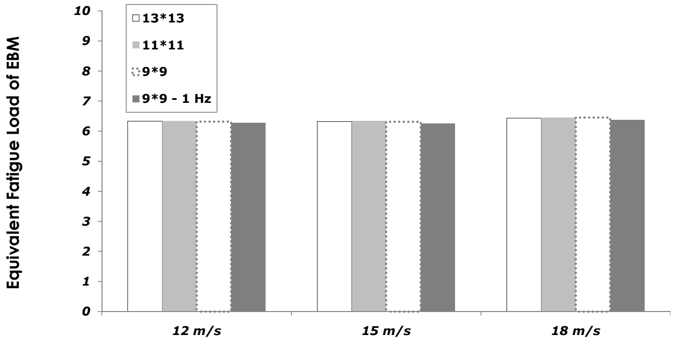

(c) Equivalent Fatigue Load of EBM

Figure 2.7: Bar charts of ensemble statistics for EBM for different wind speeds and filters.

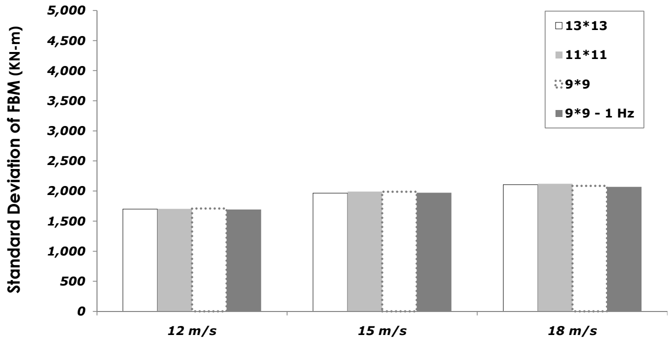

(a) Standard Deviation of FBM

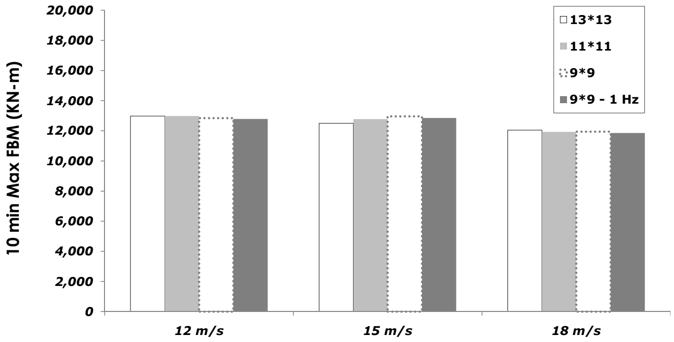

(b) 10-min Extreme of FBM

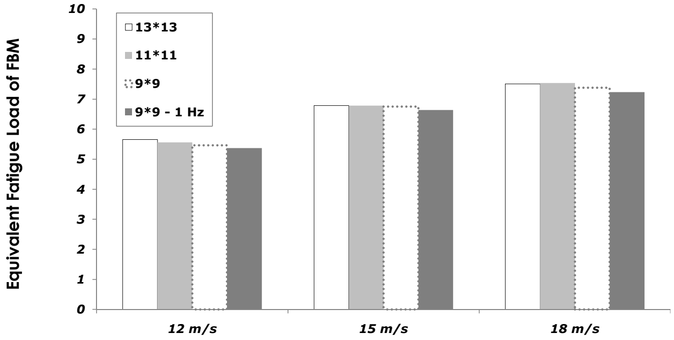

(c) Equivalent Fatigue Load of FBM

Figure 2.8: Bar charts of ensemble statistics for FBM for different wind speeds and filters.

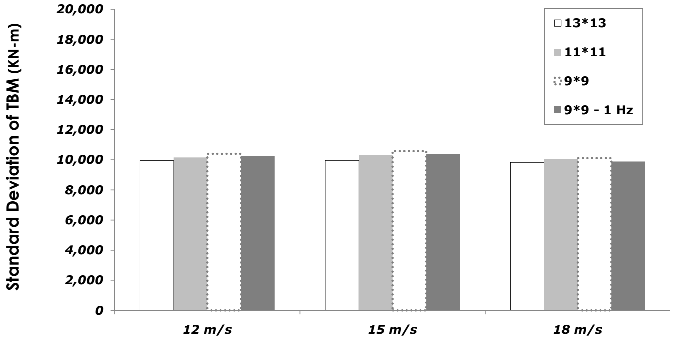

(a) Standard Deviation of TBM

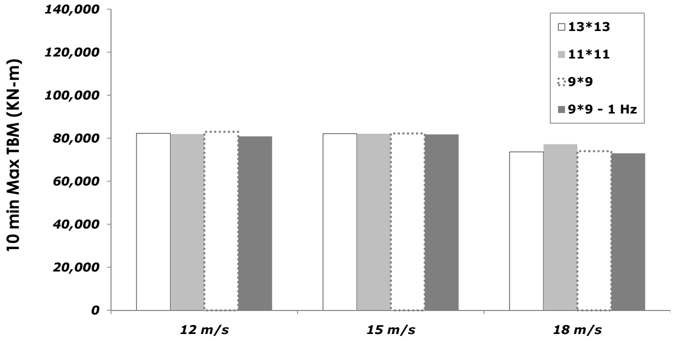

(b) 10-min Extreme of TBM

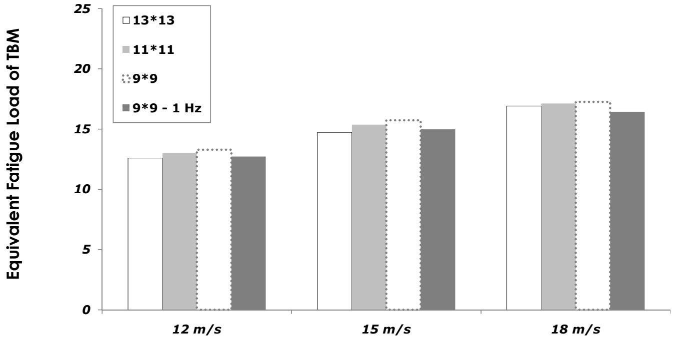

(c) Equivalent Fatigue Load of TBM

Figure 2.9: Bar charts of ensemble statistics for TBM for different wind speeds and filters.

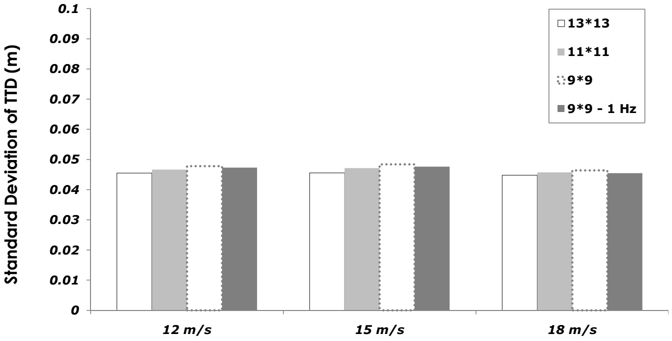

(a) Standard Deviation of TTD

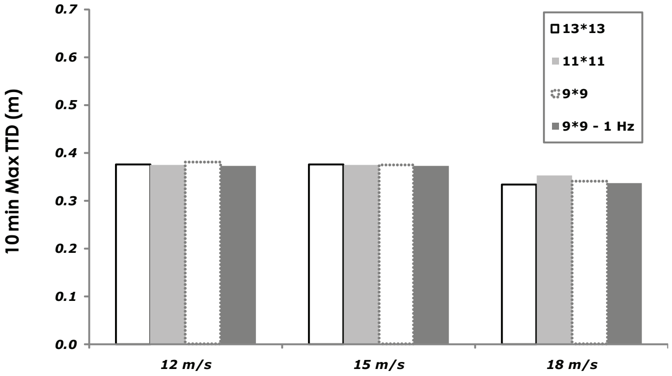

(b) 10-min Extreme of TTD

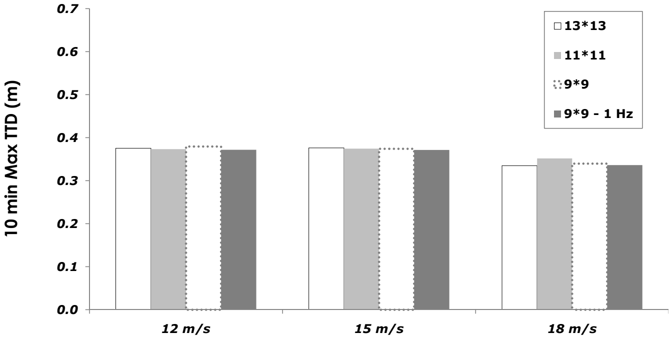

(c) Equivalent Fatigue Load of TTD

Figure 2.10: Bar charts of ensemble statistics for TTD for different wind speeds and filters.

errors in the load standard deviations for all load types.

Ensemble ten-minute extreme load estimates show slightly decreasing trends with increase in wind speed from 12 m/s to 18 m/s. This is expected since the turbine is pitch-controlled and has rated wind speed around 11.5 m/s. Loads are reduced for wind speeds above rated due to pitching of the blades. The various spatial grids and even the 9×9 grid with a 1 Hz filter do not lead to large errors in ten-minute load extremes for all load types.

Ensemble equivalent fatigue load (EFL) estimates for three of the loads studied (FBM, TBM, and TTD) show increasing trends with increase in wind speed from 12 m/s to 18 m/s. These trends with wind speed are more pronounced than for the other statistics studied—namely standard deviations and ten-minute extremes. EBM fatigue loads appear to be almost independent of wind speed. Comparing the different spatial grids, greater variation is seen for EFL than for the other statistics. FBM EFL estimates are slightly underestimated with coarser spatial grids while EFL estimates for TBM and TTD are slightly overestimated with coarser grids. Still, though variation due to spatial resolution of the inflow is greater for fatigue loads, again the various spatial grids and even the 9×9 grid with a 1 Hz filter do not lead to great differences in EFL estimates for all load types.

The preceding observations suggest that it may not be necessary to employ very fine spatial sampling while generating inflow turbulence to establish wind turbine loads for design. We conclude that a 9×9 spatial grid for our rotor may be adequate for reasonably accurate load statistics. In addition, since for all the four loads studied, the ten-minute extreme values are higher at 12 m/s wind speed than at higher wind speeds (as was also seen in a previous study [7]), further discussions on filtering will mostly focus on the inflow wind velocity time series with a mean hub-height wind speed of 12 m/s.

2.4.2 Temporal filtering of inflow turbulence

Next we study turbine load statistics on the 9×9 spatial grid that was shown to lead to small differences in load statistics compared to the 13×13 grid on our rotot plane. Our focus now is on comparing load statistics for inflow filtered at various frequencies: 16 Hz, 8 Hz, 4 Hz, 2 Hz, 1 Hz, 1/2 Hz, 1/4 Hz, and 1/8 Hz.

Figures 2.11 and 2.12 summarize various load statistics as a function of filter frequency for inflow velocity fields generated on 13×13 and 9×9 grids, respectively. The load statistics presented are normalized quantities—they represent the ratio of various statistics (including standard deviation, ten-minute extreme, and EFL) based on filtered inflow to those based on unfiltered inflow. The results represent ensemble statistics from 15 simulations and the unfiltered inflow had a ten-minute mean wind speed of 12 m/s at hub height.

In Figures 2.11 and 2.12, the 13×13 spatial sampling case with unfiltered wind serves as the target. Inflow velocity standard deviation and ten-minute extremes are within 10% of the target as long as filtering is not applied below 1 Hz; this is true even for the 9×9 grid. For all the loads, standard deviation and ten-minute extreme statistics are within 5% of the targets if filtering

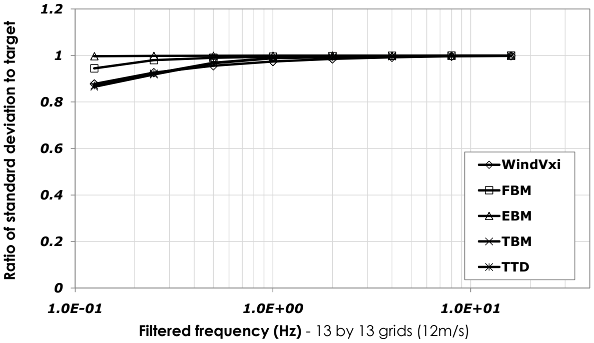

(a) Standard Deviation

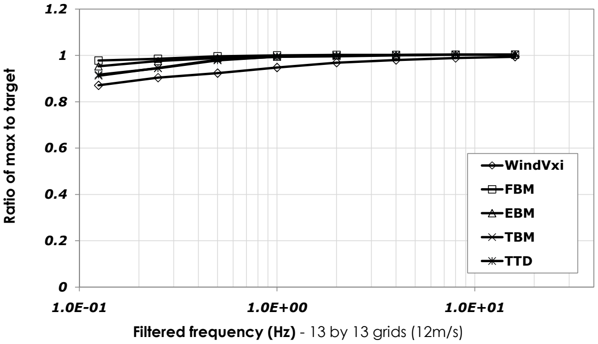

(b) 10-min Extreme

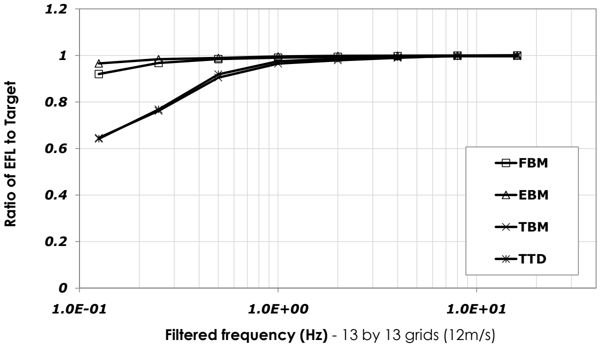

(c) Standard Deviation

Figure 2.11: Ratio of load statistics based on filtered inflow to those based on unfiltered as a function of filter frequency (based on a 13×13 grid and a ten-minute hub-height mean wind speed of 12 m/s)

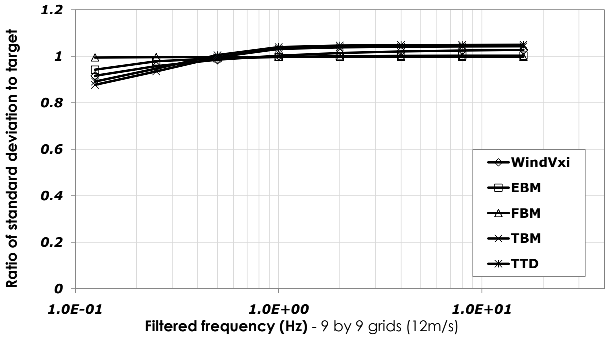

(a) Standard Deviation

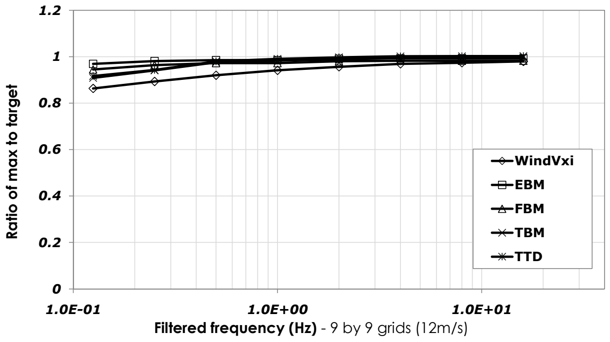

(b) 10-min Extreme

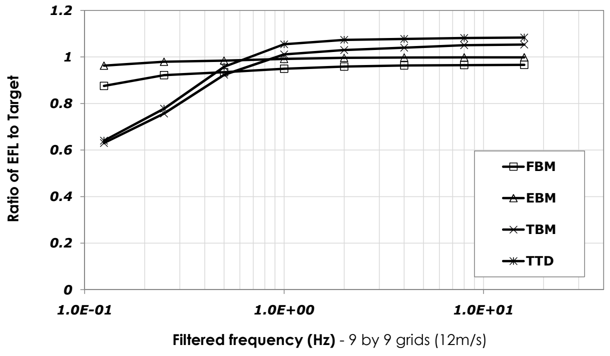

(c) Equivalent Fatigue Load

Figure 2.12: Ratio of load statistics based on filtered inflow to those based on unfiltered as a function of filter frequency (based on a 9×9 grid and a ten-minute hub-height mean wind speed of 12 m/s)

is applied at 1 Hz or higher. EFL estimates show the largest differences with filtering (when compared with the target) especially with the 9×9 grid and for the tower loads (TBM and TTD). However, with a filter at 1 Hz, the difference with respect to the target is less than 10%. In summary, a 9×9 grid for our rotor plane and 1 Hz sampling leads to inflow turbulence and load statistics (related to extremes and fatigue) that are reasonably accurate compared to a more refined 13×13 spatial grid and 32 Hz sampling.

Table 2.3: Ensemble load standard deviation estimates from 15 simulations (ten-minute mean wind speed = 12 m/s)

Grid	Standard Deviation			
	EBM	FBM	TBM	TTD
13×13 unfiltered	2,613 (KN-m)	1,701 (KN-m)	9,957 (KN-m)	0.046 (m)
9×9 filtered (1 Hz), normalized	0.997	0.996	1.031	1.039

Tables 2.3 to 2.5 show ensemble load statistics from 15 simulations for a 13×13 grid with unfiltered inflow. Ensemble load estimates for a 9×9 grid with a 1 Hz filter are also tabulated after normalizing with respect to the 13×13 grid and the unfiltered inflow. These results are for a hub-height mean wind speed of 12 m/s. Tables 2.3 to 2.5 confirm the comments made related to the results in Figs. 2.11 and 2.12. With a 9×9 spatial grid on the rotor plane and 1 Hz filter for inflow turbulence, all the load statistics are, at the very worst, only slight above 5% in error (relative to 32 Hz sampled inflow on

a 13×13 grid).

Table 2.4: Ensemble ten-minute extreme load estimates from 15 simulations (ten-minute mean wind speed = 12 m/s)

Grid	10-min extreme			
	EBM	FBM	TBM	TTD
13×13 unfiltered	5,776 (KN-m)	12,979 (KN-m)	82,295 (KN-m)	0.375 (m)
9×9 filtered (1 Hz), normalized	0.973	0.985	0.983	0.991

Table 2.5: Ensemble equivalent fatigue load estimates from 15 simulations (ten-minute mean wind speed = 12 m/s)

Grid	Equivalent fatigue load			
	EBM	FBM	TBM	TTD
13×13 unfiltered	6.333	5.656	12.585	0.052
9×9 filtered (1 Hz), normalized	0.992	0.949	1.011	1.054

2.5 Dynamic Characteristics of Turbine Loads

2.5.1 Variable-Speed Control Turbine

Time histories of the fore-aft tower bending moment (TBM) for a variable-speed wind turbine and a constant-speed wind turbine are shown in Figs. 2.13 and 2.14, respectively. These time series show a slight phase difference in the loads for the unfiltered and 1 Hz filtered inflow cases. For the same TBM loads on a constant-speed machine, no phase difference is seen in the load time series before and after filtering. The turbine in our study is a variable-speed machine. If time series on loads are studied, some differences are seen before and after filtering; this can be confirmed by the "Difference" on time series in Fig. 2.13.

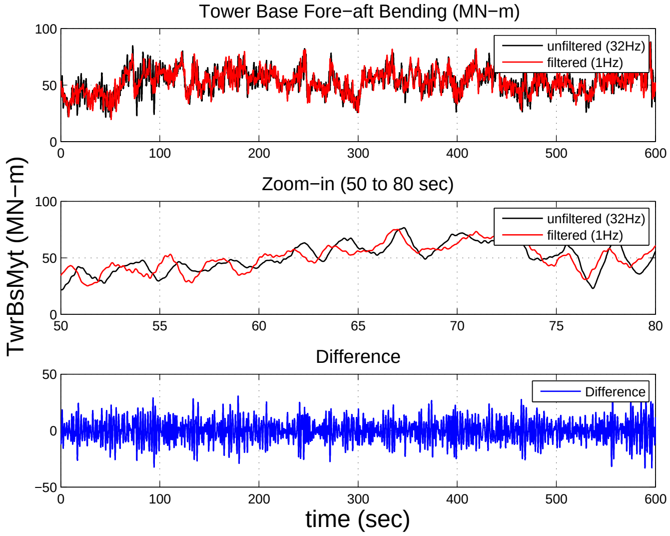

Figure 2.13: Fore-aft tower bending moment time series for a variable-speed wind turbine.

These differences are not evident for constant-speed machine. Note that the phase differences in loads are expected on variable-speed machines when considering unfiltered versus filtered inflow winds. This is because the azimuthal position of a blade that encounters an instantaneous gust at a fixed point in space will vary in general with different inflow filtering because the turbine's rotation rate might be slightly different as a result of the filtering. Even though the differences in load time series are seen for the variable-speed machine, load statistics are not significantly affected. Also, frequency-domain summaries of the loads as are possible, say, by studying power spectra are not affected by phase.

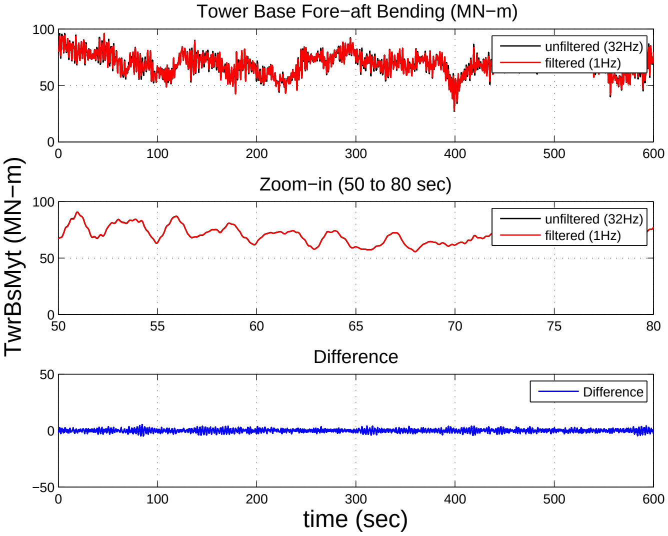

Figure 2.14: Fore-aft tower bending moment time series for a constant-speed wind turbine.

2.5.2 Power spectral density functions for turbine loads

Gravitational, inertial, and aerodynamic sources all contribute to the overall loading on wind turbine components [10]. Gravitational loading refers, for example, to the force on blades that cause periodic loading once per revolution; these forces are experienced at the rotor's rotational frequency denoted by 1P (in our case, 1P corresponds to approximately 0.2 Hz). This loading effect can be easily detected by studying the edgewise bending moment (EBM) on turbine blades. Inertial loading is caused by acceleration or deceleration of the blade rotation, due to which, centrifugal forces are caused on the blades. This centrifugal force has two components; one is spanwise and the other is in a normal direction. These latter forces influence the flapwise bending moment (FBM) on a blade. Lastly, aerodynamic loads created by the inflow affect turbine loads. It is instructive to study power spectral density (PSD) functions of the four turbine loads (FBM, EBM, TBM, and TTD) in order to understand the dynamic behavior of our wind turbine.

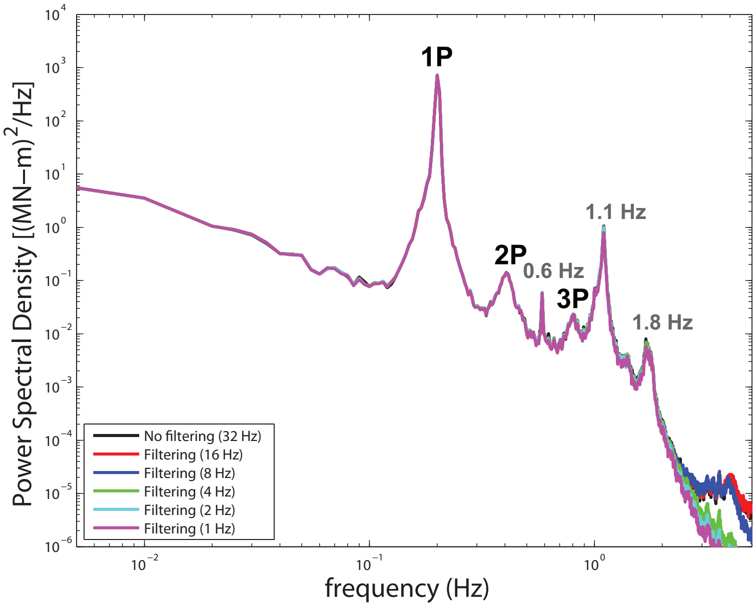

Figure 2.15: Power spectral density function for EBM from inflow simulated on a 9×9 grid and with a ten-minute mean wind speed of 12 m/s.

PSDs for EBM, FBM, TBM, and TTD, respectively, are presented in Fig. 2.15, Fig. 2.16, Fig. 2.17, and Fig. 2.18. The loads data for these PSDs were generated from a full-field inflow on a 9×9 grid with hub-height ten-minute mean wind speed of 12 m/s. Because the natural modes of vibration for our wind turbine model as specified in Table 2.2 suggest that important blade and tower vibration modes occur at frequencies below 5 Hz, log-log plots of the four PSDs were plotted only up to 5 Hz.

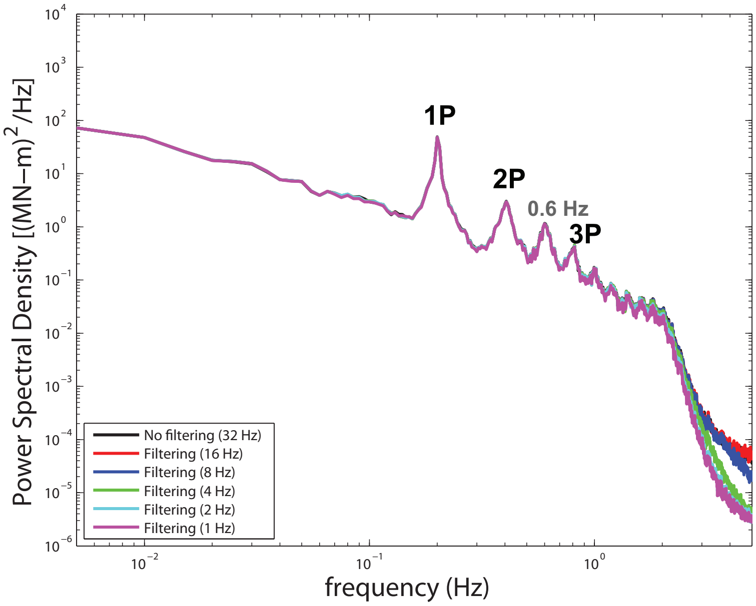

Figure 2.16: Power spectral density function for FBM from inflow simulated on a 9×9 grid and with a ten-minute mean wind speed of 12 m/s.

All the PSDs discussed here are estimated based on an ensemble of 15 simulations. Peaks in the PSDs due to the rotational frequencies of the blade (1P = 0.2 Hz, 2P, and 3P) and other important natural frequencies (such as

0.6 Hz, 1.1 Hz, 1.8 Hz, and 3.4 Hz) specified in Table 2.2 are indicated on the plots. The plots in Figs. 2.15 to 2.18 also show the PSDs derived based on filtered inflow (at various cut-off frequencies). The 1P spectral peaks and the various resonance peaks that match natural frequencies of the turbine blades and tower are easily identified and are all captured well even with filtering down to 1 Hz.

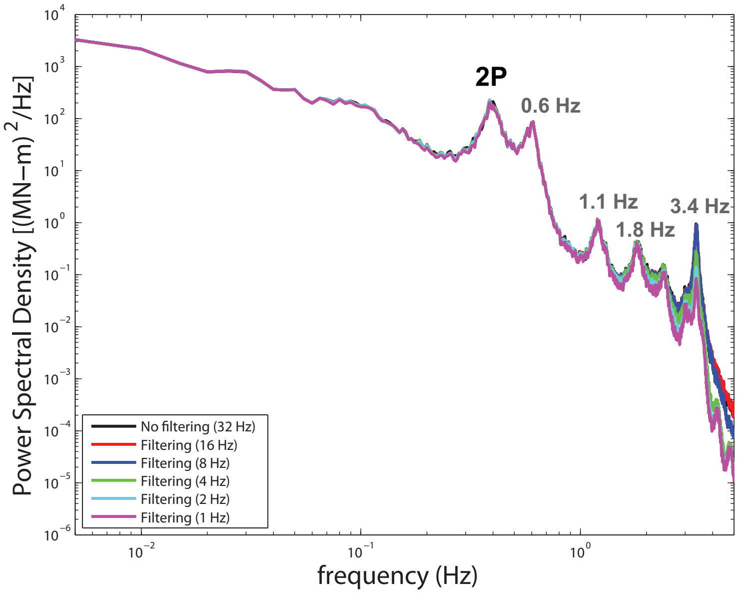

Figure 2.17: Power spectral density function for TBM from inflow simulated on a 9×9 grid and with a ten-minute mean wind speed of 12 m/s.

In the EBM PSD, the dominant peak is at 1P due to gravity forces; this fairly narrow-band power spectrum is easily verified by the regular cycles seen in EBM time series. The first edgewise bending mode frequency around 1.1 Hz is also evident, though it is far less important than the 1P peak. In the

FBM PSD, the presence of 1P, 2P, 3P, etc. peaks is obvious; these peaks occur due to rotational sampling of the inflow turbulence by the moving blades. A 0.6 Hz peak is an indication of the first flapwise blade bending mode.

Unlike the blade loads, PSDs for the fore-aft bending moment at the tower base (TBM) and the fore-aft tower top displacement shown, respectively, in Figs. 2.17 and 2.18 show largest peaks at around 0.4 Hz (close to the 2P frequency). This frequency matches the first tower bending natural frequency.

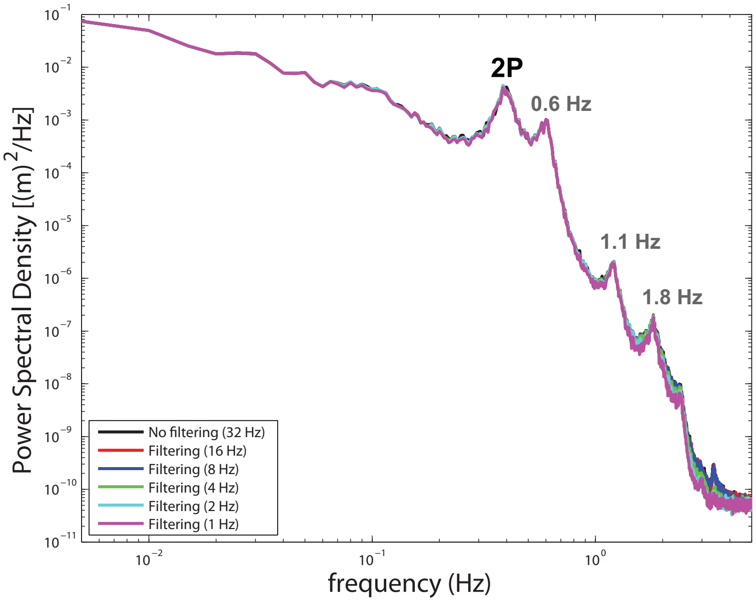

Figure 2.18: Power spectral density function for TTD from inflow simulated on a 9×9 grid and with a ten-minute mean wind speed of 12 m/s.

Studying the PSDs of the tower and blade loads helps explain why tower load statistics miss the target to a greater degree than do the blade load statistics. The PSDs clearly show that the energy (related to variance which is the area under the PSD) of the blade loads is relatively concentrated to a greater degree at the low frequencies while tower loads display peaks above 2 Hz. The dominant peaks for EBM and FBM are well captured by filtered inflow; TBM and TTD spectra show less dominant peaks and some deficient energy at a few spectral peaks.

2.5.3 Wavelet analyses of turbine loads

According to Kelley [17], time-frequency analysis using continuous wavelet transforms can help study peaks that occur coincidentally with higher-order modes that might not be detected through spectral analysis. Wavelet analysis of the loads data was performed to determine whether cutting off high frequencies in the inflow turbulence would affect turbine load characteristics in any significant way. Also, non-stationary characteristics of loads from aeroelastic simulations such as flapwise bending loads may be lost by relying on spectral analysis [17].

Figure 2.19(a),(c),(e) show results of the wavelet analysis of the flapwise bending moment (FBM) resulting from an unfiltered inflow (13×13 grid and 32 Hz sampling) and an inflow filtered at 1 Hz on a 9×9 grid (for a hub-height mean wind speed of 12 m/s). The colorbar shows FBM values in MN-m. The x-axis shows time, while the y-axis shows the time scale of the Morlet wavelet used in the analyses. At high frequencies, the time windows are narrow; while at low frequencies, the frequency windows are narrow. In other words, the long time scale “a” on the y-axis indicates low frequencies, while the short time scale indicates high frequencies.

The two wavelet plots demonstrate that there is almost no difference in the blade loads that results from filtering down to 1 Hz and using a 9×9 spatial grid for our rotor. The maximum difference in the FBM wavelet plots for the unfiltered and filtered cases is only 0.939 MN-m; peaks in time and at different scales are recovered quite well for the filtered flows.

Figure 2.19(a),(c),(e) show results of the wavelet analysis of the flapwise bending moment (FBM) resulting from an unfiltered inflow (13×13 grid and 32 Hz sampling) and an inflow filtered at 1 Hz on a 9×9 grid (for a hub-height mean wind speed of 12 m/s). The colorbar shows FBM values in MN-m. The x-axis shows time, while the y-axis shows the time scale of the Morlet wavelet used in the analyses. At high frequencies, the time windows are narrow; while at low frequencies, the frequency windows are narrow. In other words, the long time scale "a" on the y-axis indicates low frequencies, while the short time scale indicates high frequencies.

Figure 2.19(b),(d),(f) show results of the wavelet analysis of the tower base fore-aft moment (TBM) for the same filtered versus unfiltered cases as were studied for FBM. The wavelet plots show that TBM derived from unfiltered and filtered inflow also do not show great differences at low frequencies, while at higher frequencies (a=2 sec) some of the peaks are missing for the filtered case.

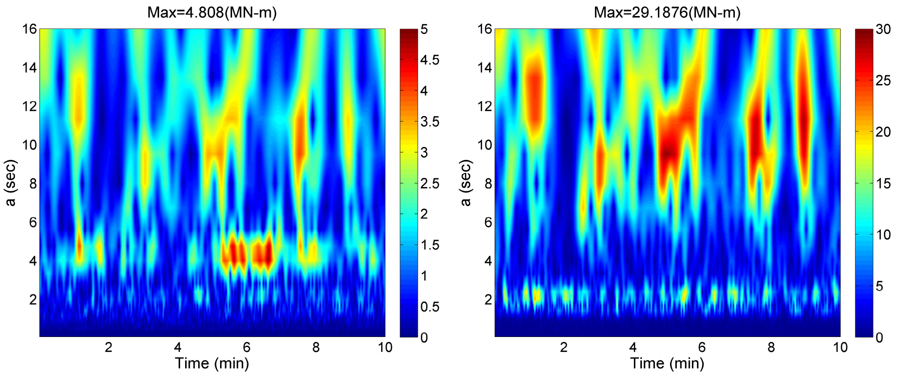

(a) FBM (unfiltered) (b) TBM (unfiltered)

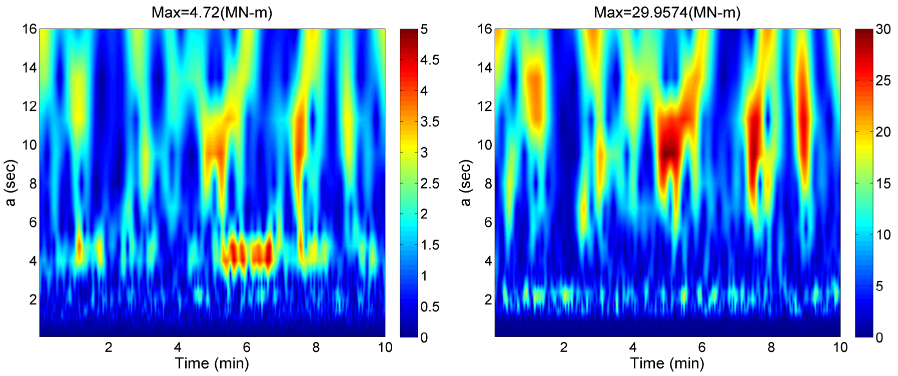

(c) FBM (filter: 1 Hz) (d) TBM (filter: 1 Hz)

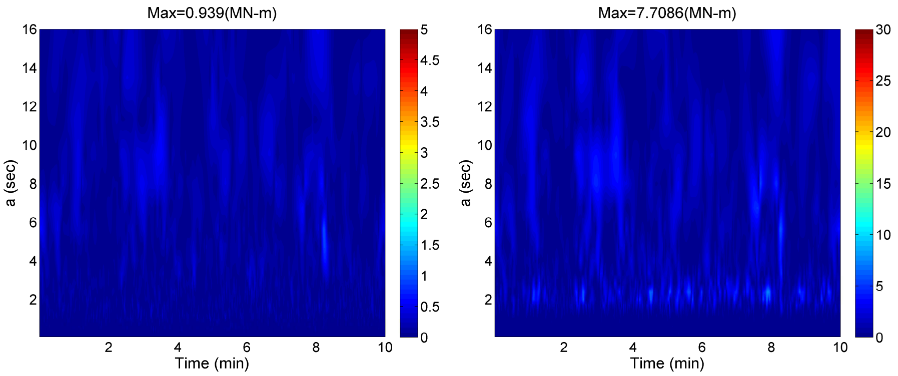

(e) Difference of FBM (f) Difference of TBM

Figure 2.19: Wavelet analysis of turbine blade and tower loads

2.6 Summary and Conclusions

Inflow turbulence was generated based on conventional Fourier-based stochastic simulations. The base inflow was filtered with various spectral cut-off frequencies to generate inflow with different spectral content, deficient in high-frequency energy. The purpose of filtering the inflow was to evaluate whether high frequencies are actually required in aeroelastic simulations. The filtered and unfiltered inflow fields were applied as input to a 5MW wind turbine model. Turbine blade and tower load time series were studied. It was found that although power spectral density functions of the filtered inflow drop considerably with greater amounts of filtering, associated load characteristics do not change significantly. In general, for all of the loads studied, it was found that 9×9 spatial grids on the rotor plane and 1 Hz sampling could be used to estimate load statistics with reasonable accuracy. Power spectra and wavelet analyses confirmed that there was no negligible losses from such filtering.

The findings from this study suggests that a grid spacing around one-tenth of the rotor diameter (10 m) and 1 Hz inflow data may be appropriate to generate from LES to allow for comparisons with conventional stochastic simulation. Such spatial and temporal resolution of the inflow should also not lead to significant errors in load statistics.

Chapter 3

Large-Eddy Simulation and Stochastic Simulation of Neutrally Stable Inflow Turbulence

3.1 Introduction

In Chapter 2, we determined adequate temporal and spatial sampling values that may be used for complex large-eddy simulation (LES). The reason we wish to generate inflow turbulence fields based on complex atmospheric simulation is because an objective of this research is to show if turbine loads based on the inflow generated from LES for neutrally stable flows do or do not differ greatly from turbulence produced by stochastic simulations. If we find that differences are small, we can then conclude that LES may be applied in studies dealing wind turbine loads. Consequently, this will then enable the wind energy industry to address specific issues in the design of wind turbines that deal with nocturnal stable boundary layer (SBL) conditions using LES.

While LES preserves most of the boundary layer characteristics by solving the nonlinear Navier-Stokes equation and the conservation of mass equations, due to the computational effort required in such simulations, less computationally intensive stochastic simulations based on Fourier techniques are more commonly used in the design of wind turbines. In contrast, stochastic simulations have limitations in modeling the stratified stable boundary layer flows that are accompanied by high wind shear and low-level jets as is the case at Great Plains sites. This is the reason why we would like to use LES that can physically generate stable boundary layer conditions by solving the nonlinear Navier-stokes equations. The present study being undertaken prior to applying LES in SBL simulations seeks to evaluate wind turbine load statistics for ideal neutral conditions that can be simulated using stochastic techniques, and then compare those statistics with those based on LES-generated inflow. First, the theoretical background of LES is briefly discussed. Second, we demonstrate how the inflow turbulence is generated based on both LES and stochastic simulation. Next, the power spectral densities and the variance of inflow turbulence generated by both techniques are reviewed. Finally, the fractal interpolation is introduced which is an inexpensive tool that is capable of improving the inflow turbulence field generated from the LES especially in deficient high-frequency energy.

3.2 Governing Equations of Large-Eddy Simulation

Large-eddy simulation (LES) is at present the most efficient technique available for high Reynolds number flow simulations, such as for atmospheric boundary layer (ABL) simulations, in which the larger scales of motion are resolved explicitly and the smaller ones are modeled. Over the past three decades, the field of LES for the ABL has evolved quite dramatically. LES has enabled researchers to probe various boundary layer flows by generating unprecedented high-resolution four-dimensional turbulence data. As a consequence, we have gained a better understanding of some fairly complex ABL phenomena. In rotation-influenced ABLs, the equations for the conservation of momentum (using the Boussinesq approximation) and temperature are:

$$\frac{\partial \tilde{u}_i}{\partial t} + \frac{\partial (\tilde{u}_i \tilde{u}_j)}{\partial x_j} = -\frac{\partial \tilde{p}}{\partial x_i} - \frac{\partial \tau_{ij}}{\partial x_i} + \delta_{i3} g \frac{(\tilde{\theta} - \left\langle \tilde{\theta} \right\rangle)}{\theta_0} + f_c \varepsilon_{ij3} \tilde{u}_j + F_i \tag{3.1}$$

$$\frac{\partial \tilde{\theta}}{\partial t} + \frac{\partial \left(\tilde{u}_j \tilde{\theta} \right)}{\partial x_j} = -\frac{\partial q_j}{\partial x_j} \tag{3.2}$$

where t refers to time; x_j is the spatial coordinate in the direction, j; u_j is the velocity component in the direction, j; θ is potential temperature; θ_0 is the reference surface potential temperature; p is the dynamic pressure; δ_{i3} is the Kronecker delta; ϵ_{ij3} is the alternating unit tensor; g is the gravitational acceleration; f_c is the Coriolis parameter; and F_i is a forcing term (e.g., geostrophic wind).

Molecular dissipation and diffusion have been neglected here since the Reynolds number of the ABL is very high and no near-ground viscous processes are resolved. Note that $\langle . \rangle$ is used to define a horizontal plane average; also the tilde (i.e.,"$\sim$") above some variables in Eqs. 3.1 and 3.2 denotes a spatial filtering operation, using a filter of characteristic width, Δ_f. These filtered equations are now amenable to numerical solution on a grid of mesh size, Δ_g, considerably larger than the smallest scale of turbulent motion (the so-called Kolmogorov scale). The effects of the unresolved scales (smaller than Δ_f)

on the evolution of $\tilde{u}_i$ and $\tilde{\theta}$ appear in the subgrid-scale (SGS) stress,τ_{ij} (in Eq. 3.1) and the SGS flux, q_j (in Eq. 3.2), respectively; these are defined as follows: $\tau_{ij} = \widetilde{u_i u_j} - \tilde{u}_i \tilde{u}_j$ and $q_j = \widetilde{u_i \theta} - \tilde{u}_i \tilde{\theta}$. Note that the SGS stress and flux quantities are unknown and must be parameterized (using a SGS model) as a function of the resolved velocity and temperature fields. Eddy viscosity models, the most popular SGS models, use the "gradient hypothesis" and formulate the SGS stress tensor (the deviatoric part) as follows [9, 21]:

$$\tau_{ij} - \frac{1}{3}\tau_{kk}\delta_{ij} = -2\nu_t \tilde{S}_{ij} \tag{3.3}$$

where S_{ij} is the resolved strain rate tensor and ν_t denotes the eddy viscosity.

From a dimensional analysis, ν_t can be interpreted as the product of a characteristic velocity scale and a characteristic length scale [9]. Different eddy-viscosity formulations basically use different velocity and length scales. The most popular eddy viscosity formulation is the Smagorinsky model [21]:

$$\nu_t = (C_s \Delta_f)^2 \left|\tilde{S}\right| \tag{3.4}$$

where C_s is the so-called Smagorinsky coefficient, which is adjusted empirically or dynamically to account for shear, stratification, and grid resolution, and $|S_{ij}|$ is the magnitude of the resolved strain rate tensor.

Similar to the SGS stresses, eddy-diffusivity models are used for the SGS heat fluxes as follows:

$$q_i = -\nu_{ht} \frac{\partial \tilde{\theta}}{\partial x_i} = -\frac{\nu_t}{\mathrm{Pr}_{SGS}} \frac{\partial \tilde{\theta}}{\partial x_i} \tag{3.5}$$

where Pr_{SGS} is the SGS Prandtl number.

The values of the Smagorinsky-type SGS model parameters, C_s and Pr_{SGS}, are well established for homogeneous isotropic turbulence [18]. However, the value of C_s is expected to decrease with increasing mean shear and stratification. This expectation has been confirmed by various recent field studies. In order to account for shear and stratification, application of the traditional eddy-viscosity model in LES of ABL flows (with strong shear near the ground and temperature-driven stratification) has traditionally involved the use of various types of wall-damping functions and stability corrections, which are either based on the phenomenological theory of turbulence or empirically derived from observational data. Similarly, a priori prescriptions exist also in the case of eddy-diffusivity SGS models.

An alternative approach is to use the "dynamic" SGS modeling approach. In this approach, one computes the value of the unknown SGS coefficients (e.g., C_s in the Smagorinsky-type eddy-viscosity models) dynamically at every time and every position in the flow. By looking at the dynamics of the flow at two different resolved scales and assuming scale similarity as well as scale invariance of the model coefficient, one can optimize its value [8, 18]. Thus, the dynamic model avoids the need for a priori specification and tuning of the coefficient because it is evaluated directly from the resolved scales in an LES. Recently, Basu and Porté-Agel [5] proposed a refined dynamic modeling approach (called the "locally-averaged scale-dependent dynamic" or LASDD SGS modeling approach) for ABL simulations. The potential of the

LASDD SGS model was demonstrated in large-eddy simulations of the neutral boundary layer [3], of the stable boundary layer [5], and of a complete diurnal cycle [6]. In the present study, we utilize the LASDD model to generate neutral boundary layer inflow conditions for wind turbine load calculations using an aeroelastic model.

3.3 LES and Stochastic Simulation of Inflow Turbulence

In atmospheric large-eddy simulations, idealized or observed soundings (i.e., 1-D vertical profiles) of wind speed and other environmental variables (such as temperature, moisture, etc.) in conjunction with small-scale 3-D perturbations (random noise) are typically used to generate initialization fields. With the help of the Navier-Stokes equations (Eq. 3.1), these fields are then evolved in time under the constraints of certain large-scale forcing terms (e.g., geostrophic wind) and boundary conditions (e.g., prescribed land-surface temperature is often used as the lower boundary condition). Usually, it takes about an hour of simulation (depending on the characteristics of the boundary layer to be simulated) to generate realistic turbulence (e.g., for reasonable representation of the inertial range of spectra). However, it can take a few hours of simulation to generate quasi-steady state boundary layer conditions. For realistic neutral boundary layer simulations, one needs to run an LES code for O(12) hours to reach quasi-steady state conditions.

High-resolution LES runs are computationally very expensive, especially for durations of O(12) physical hours. For this reason, in this research, we carry out the simulations in two phases (see Fig. 3.1). In Phase I, coarse runs (with a grid resolution of 20 m) of 12-hour duration are performed using a time step of 0.2 seconds. Then, in Phase II, the final 3-D fields from the phase I simulations are used as initial fields and new simulations are run for 30 minutes (with a time step of 0.1 seconds). In order to create higher resolution (finer than 20 m) LES data, we first apply a cubic spline interpolation to the final 3-D fields of the Phase I simulations to produce 13.3 m resolution initial fields. Full-field wind files for 3-D velocity components are output from the last 15 minutes of these 30-minute Phase II simulations at a frequency of 2.5 Hz (i.e., every 0.4 seconds). For both phases of our simulations, we kept a fixed domain size of 800 m × 800 m × 1,260 m.

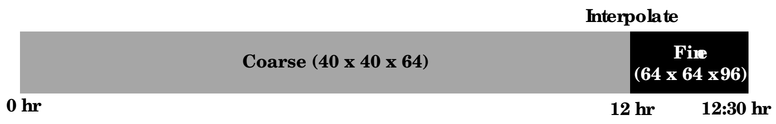

Figure 3.1: Two phases of the LES flow generation.

Fig 3.2 shows a 180 m × 180 m (y-z plane) slice of the longitudinal velocity (U) taken at one time instant from the last 15-minute time history segment of the simulated wind field (with a grid resolution of 13.3 m); also shown are the 15-min time series for U versus vertical elevation (z) for points laterally separated by 150 m. In this study, we systematically varied geostrophic winds (a large-scale forcing term related to mesoscale pressure gradient force) to obtain various hub-height wind speeds.

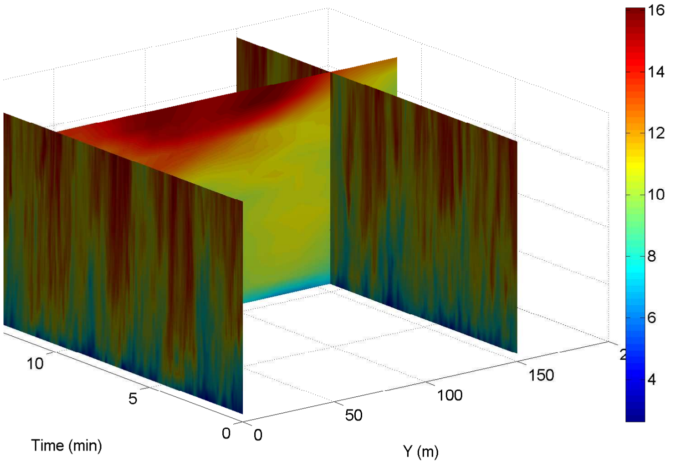

Figure 3.2: Slice of the last 15 minutes generated from LES: phase II longitudinal velocity wind field

In addition, three sets of LES were generated for each geostrophic wind case. After generating these wind fields, the 800 m × 800 m × 1,260 m domain was sliced into 5 pieces in the y direction yielding a total number of 15 cases covering (lateral) rotor planes. In addition, since the w-components were generated in a staggered form vertically where they were spaced between the vertical grid points of the u and v-components, the w-components were interpolated to the grid points of u and v-components. Then, the entire turbulence field was interpolated to the same grid points that were used in generating the NBL inflow with stochastic simulations. In order to provide neutral boundary layer flows from stochastic simulations whose effects on turbine loads could be directly compared with the neutral boundary layer flows generated from LES, the Fourier-based stochastic turbulence simulation code, TurbSim, was used together with target turbulence power spectra and coherence functions (the

Kaimal model). The rotor plane of the selected 5MW turbine, with a rotor diameter of 126 m, was represented as a 13 × 13 grid that covers a square area of side 160 m, centered at the rotor hub. A time-step of 0.4 seconds was used in the NBL flow simulations to match the time step from LES. Note that the resultant of u and v-component wind speed at hub height (90 m) for the LES case was matched to the hub-height mean wind speed of the TurbSim simulations. A total of 15 simulations were produced and compared with the LES results.

The main finding drawn from the turbulence simulation is that the inflow generated from LES is lacking in high-frequency energy while the low-frequency energy is similar to the wind field produced by TurbSim.

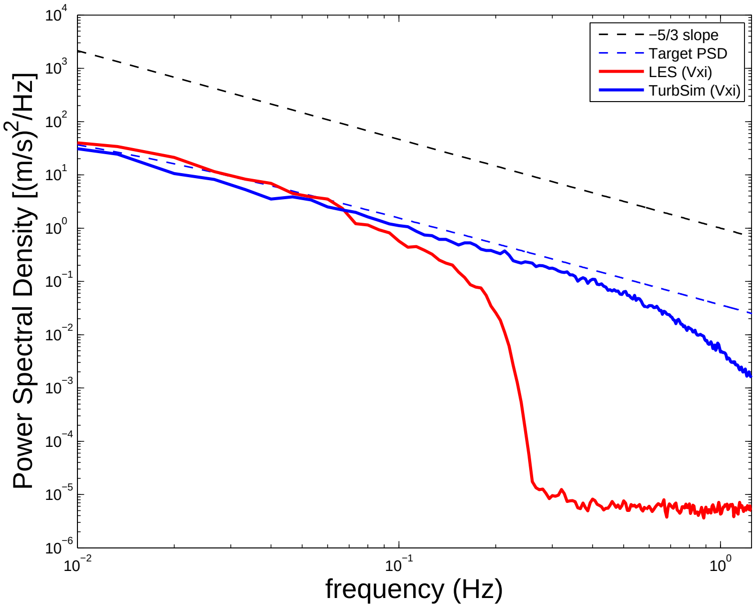

Figure 3.3: Power spectral densities of inflow turbulence

Figure 3.3 shows PSDs of the hub-height inflow turbulence estimated from flows generated by LES and TurbSim. Obvious difference in the PSDs are seen above 0.1 Hz where the power of the LES inflow drops significantly. The inflow generated by TurbSim with a sampling rate of 2.5 Hz also loses its energy relative to the target above 0.5 Hz. Both PSDs of LES and TurbSim follow the Kolmogorov slope of -5/3 before the energy reduces from the target.

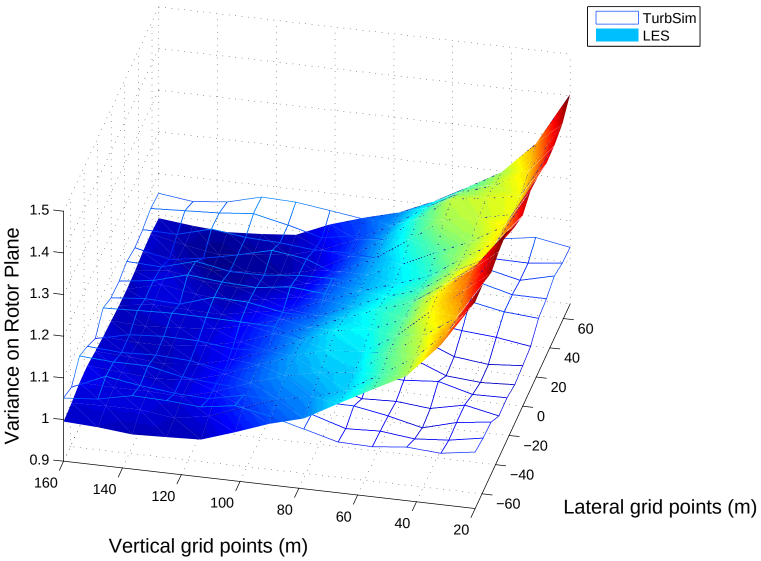

Figure 3.4: 3-D Variance of inflow turbulence across the rotor plane

Figure 3.4 shows a 3-D plot of variance of inflow turbulence across the rotor plane. The target variance in TurbSim is kept as constant for the entire rotor plane although this is not physically realistic. Large-eddy simulation generates turbulence at the surface and transports it upwards in neutral flows. As a result, variance and fluxes are higher near the surface and will decrease monotonically with height. Moreover, the variance and fluxes should be zero at the top of boundary layers (BL). Figure 3.4 clearly demonstrates that LES is capturing the correct behavior of BL characteristics. Near the hub height (90 m) of our turbine model, the variance of LES and TurbSim match reasonably well. However, while the variance from TurbSim is (by intent) not changing over the entire rotor plane, the variance from LES has higher values close to the ground (20 m) and lower values above 90 m.

To evaluate the LES of neutral boundary flow (NBL) by comparing the loads from LES flows with those form TurbSim (stochastic simulator), we would like to modify any differences in inflow in reasonable ways. Though there are noted differences in inflow variance from LES versus TurbSim over the rotor plane, this difference is preserved since LES is more realistic. The main area chosen for improvement is targeted at enhancing the high-frequency energy that is lacking in LES. The next section describes a useful technique that enables LES to address augmenting this high-frequency energy.

3.4 Fractal Interpolation of Large-Eddy Simulations

In this study, for large-eddy simulations we used grid resolutions of O(10) m. Since spatial and (implicit) temporal filtering operations are intimately related in LES, the grid resolution basically dictated the level of high-frequency content realized in the generated time series. The LES runs with temporal frequencies of O(>2.4) Hz had minimal energy, as would be anticipated. However, in using TurbSim with the identical temporal frequency of

2.4 Hz for neutral conditions, the generated velocity time-series showed additional energy at higher frequencies. Simulation of turbulence time series with higher frequency using a large-eddy model would require a grid-resolution with smaller O(0.1) m. At the present time, this is a computationally daunting task.

For such reasons, instead of performing computationally expensive high-resolution large-eddy simulations, we consider the possibility of enhancing the high-frequency content of coarse-resolution LES data by using a so-called fractal interpolation technique (FIT). FIT is an iterative affine mapping procedure that may be used to construct synthetic deterministic small-scale fields from a few given large-scale interpolating points [4].

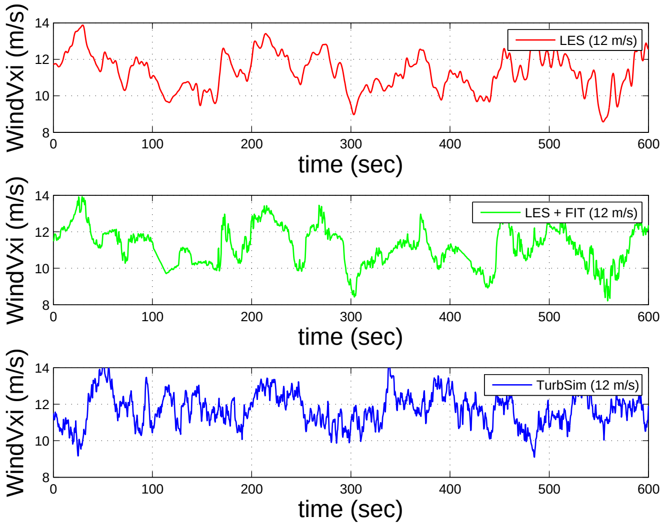

Figure 3.5: Time-histories of inflow turbulence with FIT

In addition, FIT is computationally very inexpensive and, more importantly, FIT preserves the higher-order moments and non-Gaussian probability density function of the velocity increments [4].

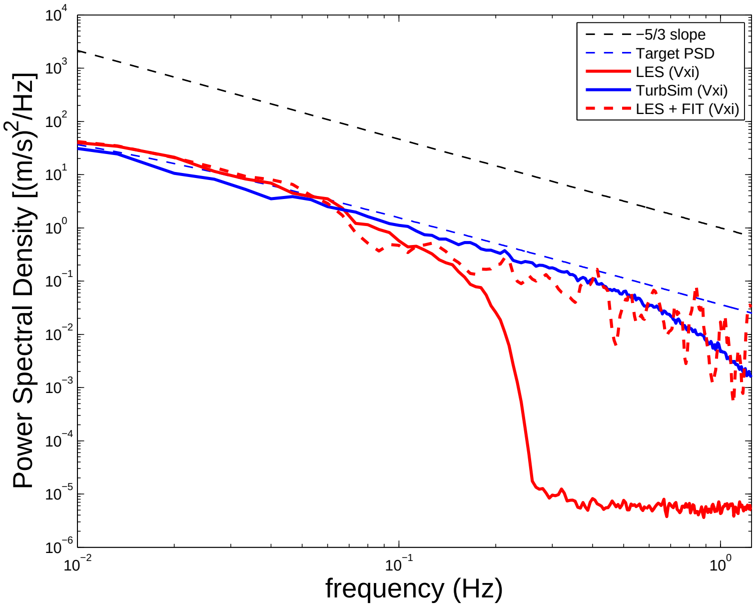

Figure 3.6: Power spectral densities of inflow turbulence with FIT

Figure 3.5 shows the result of FIT applied to a time series of wind inflow. The red line represents the case when only LES is applied. The green line corresponds to the time series produced by applying FIT to LES-generated data. Finally, the blue line shows the time series of the longitudinal wind component generated using TurbSim. It can be seen that FIT adds high-frequency content that corresponds to the small fluctuations shown in the green time series; this improves the LES time series.

Although these small fluctuations can be rapidly observed in the time series in a relative sense, it is more instructive to study the improvement at high frequencies by reviewing turbulence power spectral densities in the frequency domain. The red-dotted line in Fig. 3.6 shows the case when FIT is applied to LES. This figure reveals that the LES-generated data can have comparable inflow turbulence to the TurbSim-generated full field by the introduction of FIT.

3.5 Summary

This chapter introduced the background of Large-Eddy Simulation (LES) which is widely used in atmospheric boundary layer simulations. While LES preserves most of the boundary layer characteristics by solving the nonlinear Navier-Stokes equation and the conservation of mass equation, due to the computational effort required in such simulations, stochastic simulations based on Fourier techniques are more commonly used in the design of wind turbines. In contrast, stochastic simulations have limitations in modeling the stratified stable boundary layer flows that are accompanied by interesting conditions such high wind shear and events such as low-level jets common at Great Plains sites. A goal of this study is to compare the turbine loads under the influence of LES-generated wind and stochastic inflow. To understand the difference and optimize the LES data, we focused on the theoretically ideal (near-neutral) case of boundary layer conditions. In simulating the inflow turbulence field with LES, we referred to the results in Chapter 2 on desired temporal resolution for accurate load statistics and used a coarse time step of 0.4 sec.

In general, the LES flow fields were found to lack high-frequency energy compared to the stochastic simulation of NBL. In order to compare in a consistent way flows from LES and TurbSim and resulting extreme and fatigue loads in Chapter 4, the inflow turbulence of LES was modified to resolve high-frequency turbulence by employing a technique called fractal interpolation.

It was shown that such fractal interpolation introduces significant portions of high-frequency energy in inflow turbulence and leads to a comparable level to that expected for neutral conditions. Therefore, for the turbine load studies in Chapter 4, fractal interpolation will be applied to the full-field flows generated by LES.

Chapter 4

Extreme and Fatigue Wind Turbine Loads for LES and Stochastic Simulations

4.1 Introduction

We now use the inflow turbulence generated by LES and TurbSim as discussed in Chapter 3 to study turbine loads. Edgewise and flapwise bending moment are studied for the blade loads. Tower fore-aft bending moment at the base and tower top fore-aft displacement are studied for the tower loads. We first study load statistics for three different hub-height wind speeds. Based on the findings from this study on turbine load statistics, subsequent sections focus on only one wind speed while studying turbine loads. Power spectral densities are studied to understand dynamic characteristics of the turbine loads. Then, based on the rainflow cycle-counting algorithm briefly described in Section 4.3.1, fatigue stress range histograms and equivalent fatigue loads are estimated for alternative inflow turbulence fields. Finally, short-term load probability distributions of turbine load extremes are evaluated. One-minute block maxima from the time series are used to estimate short-term load distribution that can be useful in evaluating design load cases for wind turbines.

4.2 Turbine Loads under Neutral Inflow Turbulence

4.2.1 Turbine Load Statistics

We study turbine load statistics for the various inflow fields generated by different simulation techniques. These inflow fields are based on three different simulation models: LES, LES with FIT, and TurbSim; and three different ten-minute mean hub-height wind speeds: 12 m/s, 15 m/s, and 17 m/s. We are interested in the ten-minute extreme, the ten-minute mean, and the standard deviation for four different turbine loads (EBM, FBM, TBM, and TTD). A total of fifteen simulations were used for the turbine load calculations with each of the inflow fields. The results of these simulations are represented in box plots. These plots are also referred to as box-and-whisker diagrams and were first introduced by Tukey [22]. Quartiles that represent the 25% (lower quartile), 50% (median), and the 75% (upper quartile) are extracted from the data set; these quartiles form the box. The box plots illustrated in Figs. 4.1 to 4.12 identify the maximum and minimum values of the relevant statistic (extreme, mean, or standard deviation from 15 simulations) with whiskers. Figures 4.1 to 4.12 summarize load statistics represented by these box plots. Each figure summarizes statistics for the three inflow options (LES, LES + FIT, TurbSim) and the three wind speeds. The red box represents the LES case; the green box represents the case for LES inflow with fractal interpolation; and the blue box represents the TurbSim case.

FBM, TBM, and TTD, which are relatively more sensitive to the inflow than EBM, are seen to have higher standard deviations with increased

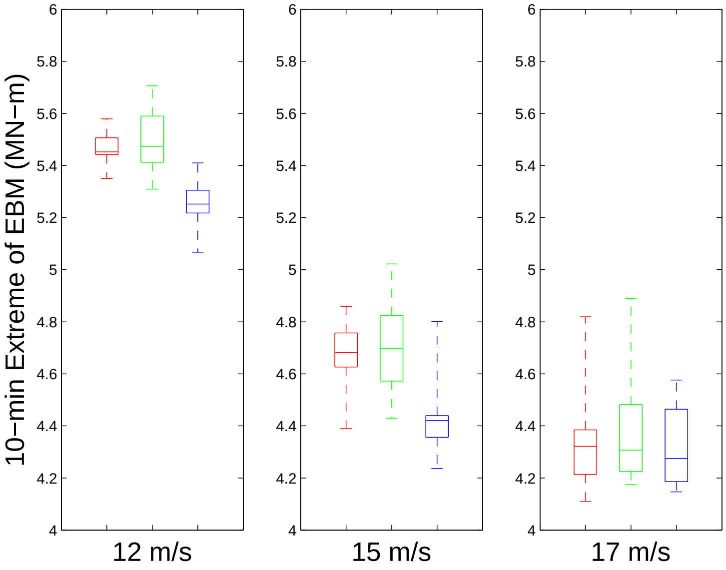

Figure 4.1: Box plot for 10-min extreme of EBM.

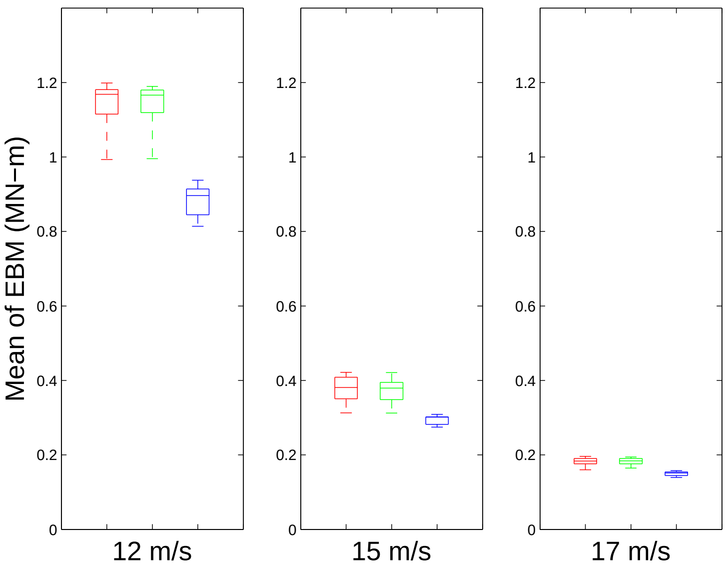

Figure 4.2: Box plot for Mean of EBM.

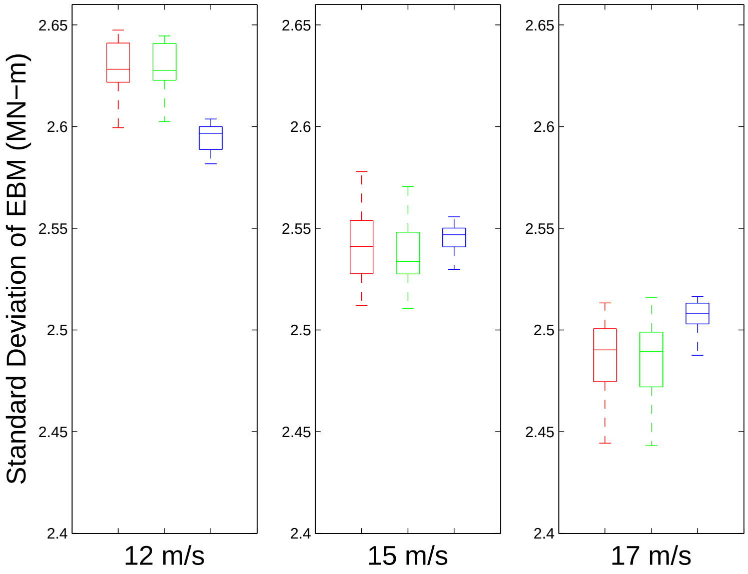

Figure 4.3: Box plot for Standard Deviation of EBM.

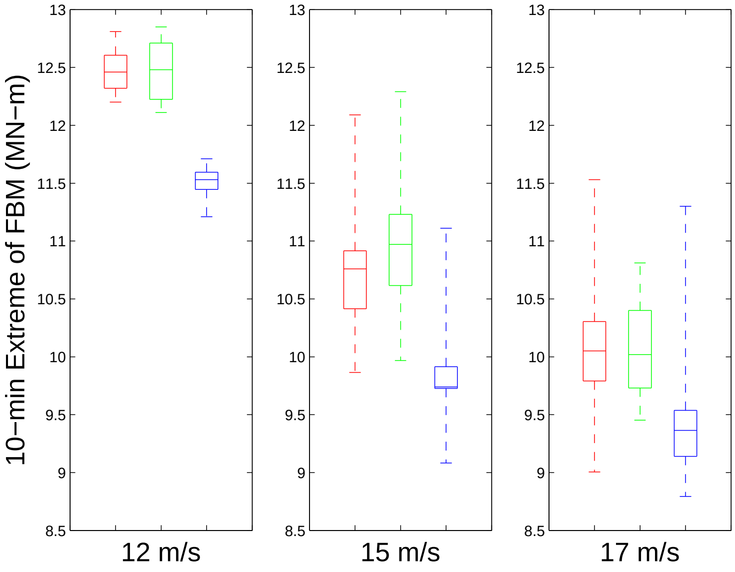

Figure 4.4: Box plot for 10-min extreme of FBM.

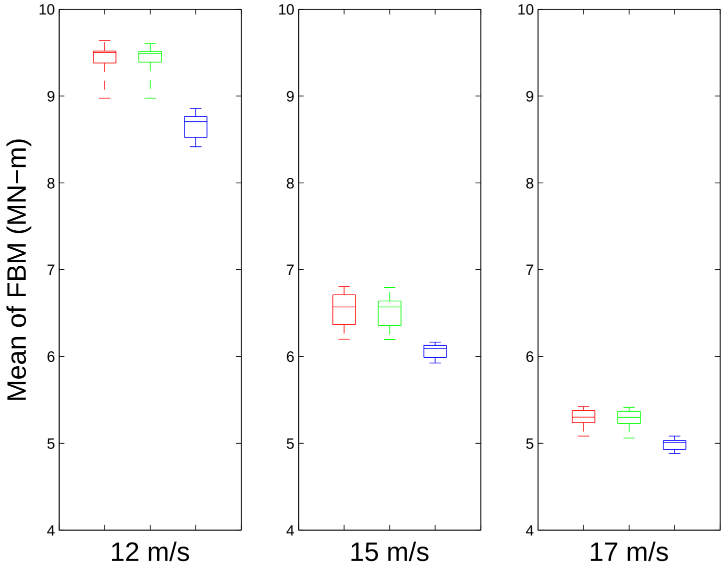

Figure 4.5: Box plot for Mean of FBM.

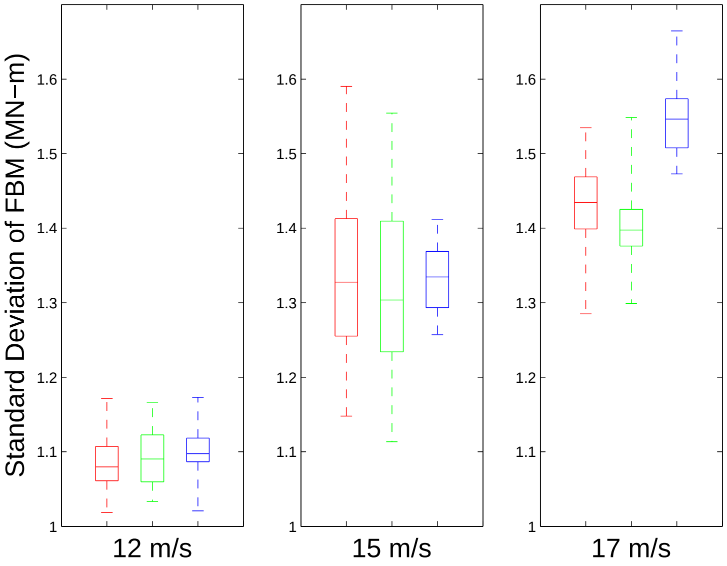

Figure 4.6: Box plot for Standard Deviation of FBM.

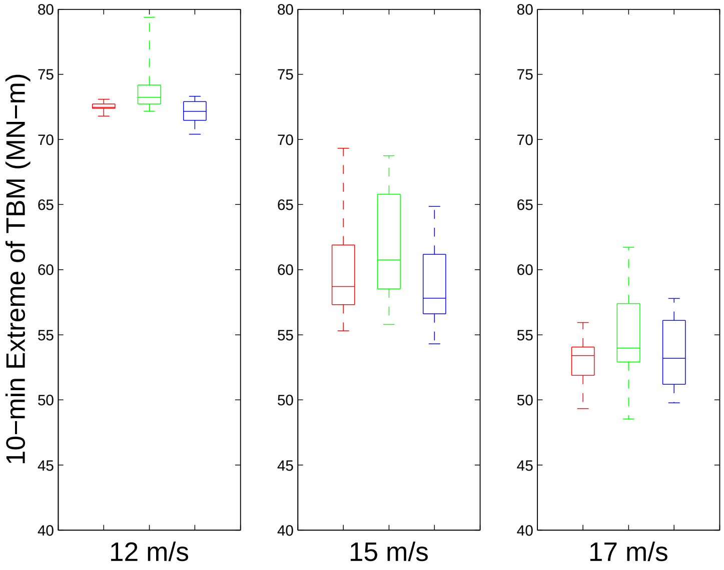

Figure 4.7: Box plot for 10-min extreme of TBM.

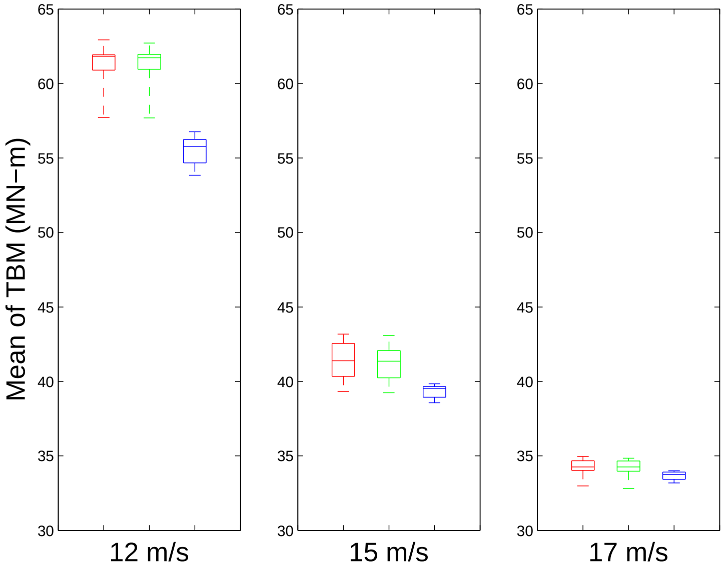

Figure 4.8: Box plot for Mean of TBM.

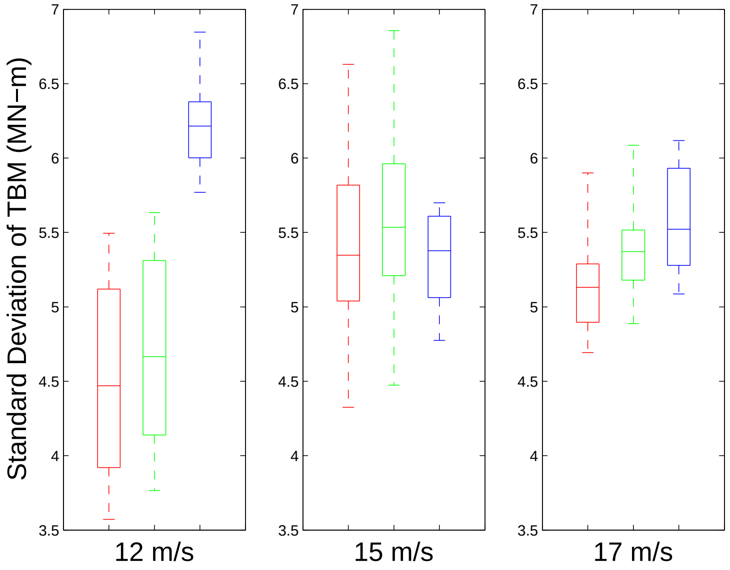

Figure 4.9: Box plot for Standard Deviation of TBM.

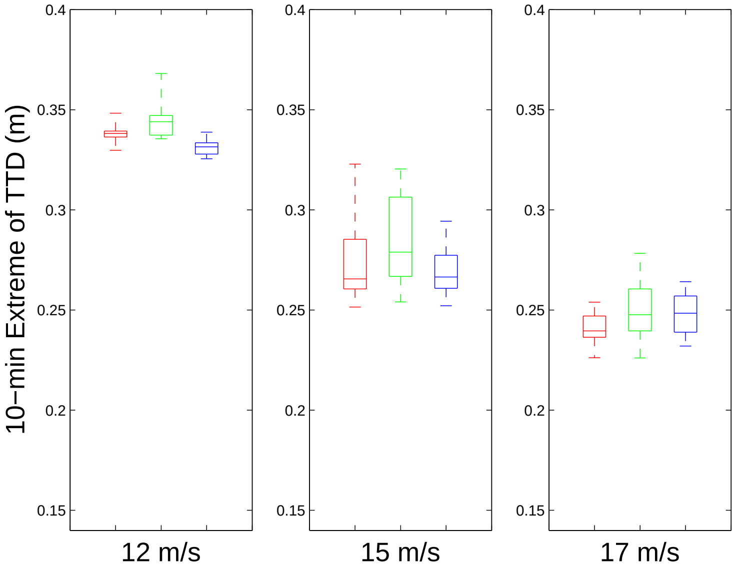

Figure 4.10: Box plot for 10-min extreme of TTD.

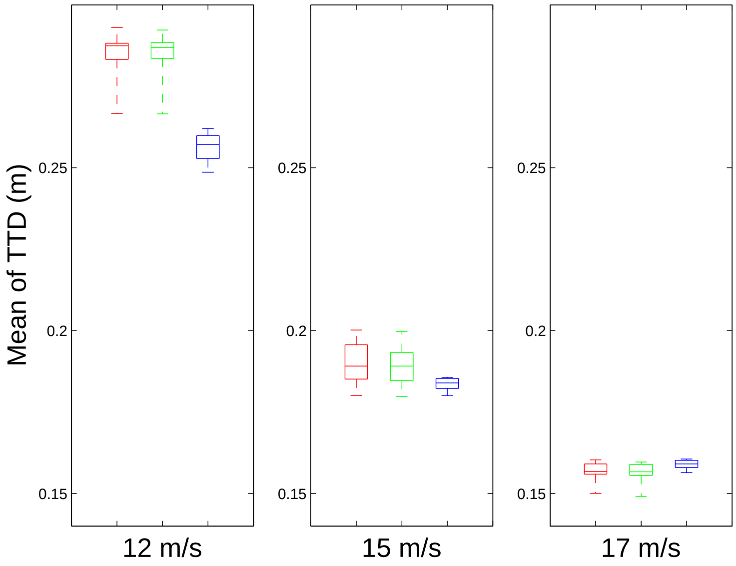

Figure 4.11: Box plot for Mean of TTD.

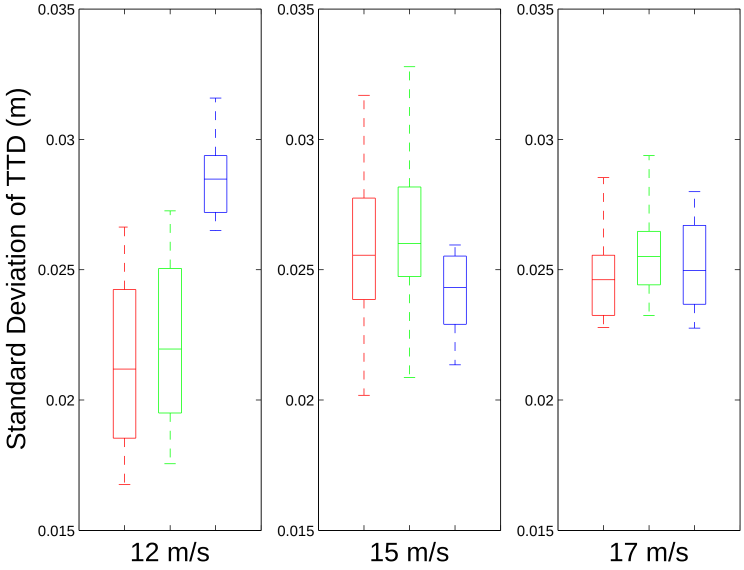

Figure 4.12: Box plot for Standard Deviation of TTD.

Table 4.1: Ensemble estimates of load standard deviation.

Wind Speed	Simulation Type	Standard deviation				
		Vxi (m/s)	FBM (MN-m)	EBM (MN-m)	TBM (MN-m)	TTD (m)
12 m/s	LES	1.077	1.086	2.629	4.493	0.021
	LES+FIT	1.146	1.094	2.629	4.696	0.022
	TurbSim	1.018	1.102	2.594	6.231	0.029
15 m/s	LES	1.570	1.340	2.540	5.418	0.026
	LES+FIT	1.653	1.329	2.538	5.633	0.026
	TurbSim	1.466	1.333	2.545	5.310	0.024
17 m/s	LES	1.796	1.433	2.487	5.167	0.025
	LES+FIT	1.189	1.409	2.485	5.408	0.026
	TurbSim	1.771	1.547	2.506	5.587	0.025

wind speeds. Ten-minute extreme loads and mean values for all four load measures and inflow simulation options suggest that the inflow conditions associated with the hub-height wind speed of 12 m/s bring about the largest loads. These results are understandable since turbine loads generally decrease as wind speeds exceed the rated wind speed due to pitch control actions. In a previous research with the identical 5MW wind turbine model [7], the wind speed bin closest to 12 m/s had large loads too as in this study. As a result, subsequent sections will focus only on loads from inflow fields with a hub-height mean wind speed of 12 m/s.

Tables 4.1 and 4.2 show the absolute values of the ensemble statistics (standard deviation, ten-minute extreme, and ten-minute mean values) from

Table 4.2: Ensemble estimates of 10-min mean and extreme values.

Wind Speed	Simulation Type	10-min mean				
		Vxi (m/s)	FBM (MN-m)	EBM (MN-m)	TBM (MN-m)	TTD (m)
12 m/s	LES	11.807	9.428	1.141	61.288	0.285
	LES+FIT	11.800	9.422	1.140	61.250	0.285
	TurbSim	11.864	8.661	0.833	55.502	0.256
15 m/s	LES	14.973	6.537	0.377	41.432	0.190
	LES+FIT	15.015	6.510	0.373	41.252	0.189
	TurbSim	14.952	6.059	0.294	39.295	0.183
17 m/s	LES	17.436	5.292	0.182	34.203	0.156
	LES+FIT	17.389	5.289	0.182	34.138	0.156
	TurbSim	17.446	4.984	0.150	33.660	0.159

Wind Speed	Simulation Type	10-min extreme				
		Vxi (m/s)	FBM (MN-m)	EBM (MN-m)	TBM (MN-m)	TTD (m)
12 m/s	LES	15.205	2.483	5.461	72.525	0.337
	LES+FIT	16.113	12.472	5.494	73.739	0.344
	TurbSim	14.768	11.506	5.261	72.125	0.331
15 m/s	LES	19.893	10.705	4.677	60.157	0.275
	LES+FIT	21.104	10.963	4.712	61.874	0.285
	TurbSim	19.187	9.830	4.421	58.829	0.269
17 m/s	LES	23.147	10.095	4.346	60.157	0.241
	LES+FIT	24.012	10.077	4.392	61.874	0.251
	TurbSim	22.677	9.476	4.333	58.829	0.248

15 simulations. As was seen in Figures 4.1 to 4.12, Tables 4.1 and 4.2 confirm that the ten-minute mean and ten-minute extreme loads decrease with increasing wind speed above 12 m/s; the standard deviation of the various loads shows no obvious trends. For all wind speeds and for all loads, the load statistics are fairly consistent for all three inflow field options.

4.2.2 Power spectral densities of turbine loads

Power spectral densities (PSD) of turbine loads that result from inflow turbulence generated by LES, LES with FIT, and TurbSim are plotted in Figs. 4.13 to 4.15. The edgewise bending moment shows a dominant peak at 1P (0.2 Hz) corresponding to the rotational frequency of our turbine model and some smaller peaks at higher frequencies. The peaks at 0.6 Hz and 1.1 Hz match the natural frequencies of the 1^{st} mode of flapwise bending moment and the edgewise bending moment of the blades.

On studying the PSD of EBM in Fig. 4.13, one can see that although there is some energy loss in the PSD for LES and PSD for LES with FIT at low frequencies, the dominant (1P) peak matches that in the PSD for TurbSim quite well.

The FBM PSD for LES inflow turbulence shown in Fig. 4.14 matches the larger PSD peaks for the inflow turbulence of TurbSim satisfactorily even without applying fractal interpolation. There is slight energy loss at low frequencies but all the peaks shown (such as at 1P, 2P, and 3P) are quite close together for all the inflow simulation options.

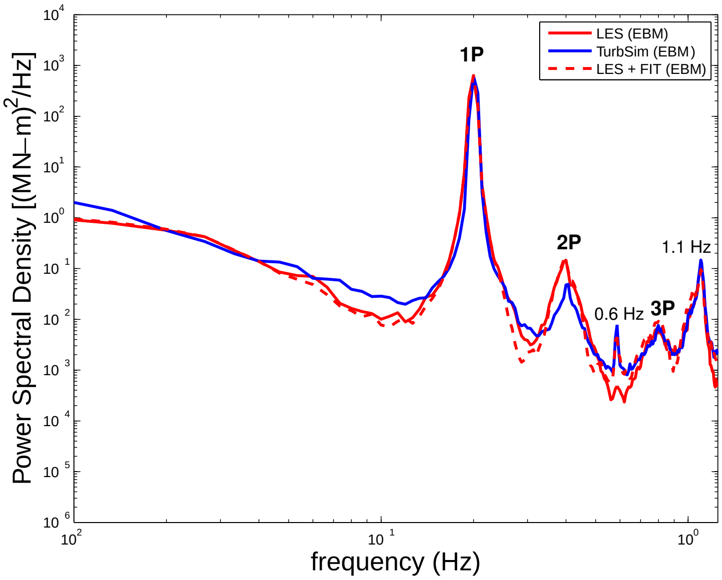

Figure 4.13: Power spectral densities of EBM.

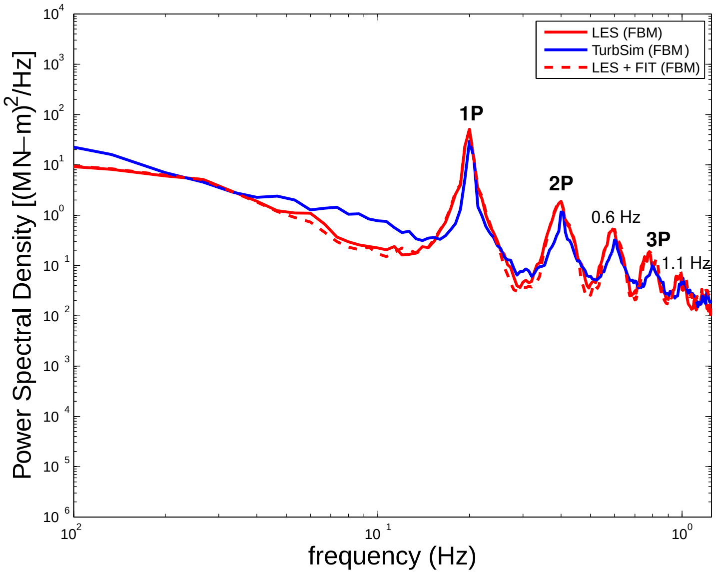

Figure 4.14: Power spectral densities of FBM.

While the blade loads under inflow turbulence generated by LES preserved the important peaks in the PSDs quite well, the tower loads (TBM) with LES inflow miss the natural frequency of the 1^{st} tower fore-aft bending mode at 0.4 Hz as can be seen in Fig. 4.15. Since this first peak makes an important contribution to the overall energy content, this deficit can lead to errors in tower load estimation. However, fractal interpolation recovers much of the missing energy between 0.4 Hz and 0.8 Hz.

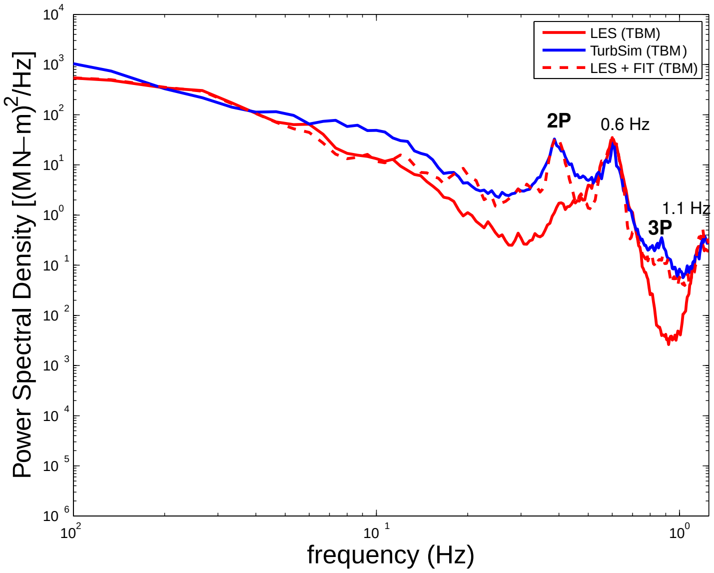

Figure 4.15: Power spectral densities of TBM.

4.3 Fatigue Load Estimation

4.3.1 Theoretical Background

Stress or load cycle histograms can be established from time series of wind turbine loads by various means including the rainflow cycle counting algorithm [2]. Rainflow cycle counting is one of the common methods used to count the number of cycles in an irregular load or stress time history. Such cycle counts can be carried out for any type of time series; this is done in the time domain. Stress cycles or strain cycles can be used in obtaining histograms that form the basis for fatigue load estimation.

The fatigue life of turbine components is usually estimated in terms of cumulative damage [24]. The cumulative damage in turbine components may be calculated based on the assumption of linear cumulative damage. This assumption forms the basis of the well-known Palmgren-Miner's linear damage rule. The total damage can be expressed as the cumulative damage from various load cycles. Damage in any single cycle is proportional to the stress range amplitude, S, to the m^{th} power, where m is called the Wohler exponent. In addition, the material parameter, K, is proportional to the number of cycles the material can resist prior to failure. If the number of cycles to failure, N_F, is used, Miner's rule can be expressed as follows:

$$N_F \cdot S^m = K \tag{4.1}$$

In dealing with variable-amplitude time series, the Rainflow cycle-counting algorithm [2] is used to numerically extract different stress cycles,

S_i. The number of counted stress cycles, N, is the number of full cycles plus the number of half cycles multiplied by 0.5. Then Eq. 4.1 can be expressed in a different format with the introduction of a parameter called the damage fraction, D, which can vary between zero and unity; $D = 1$ indicates fatigue failure. Miner's rule can be expressed as follows:

$$D = \frac{\sum\limits_{i=1}^{N} S_i^m}{K} \tag{4.2}$$

In a similar fashion, the damage can be expressed using an equivalent fatigue load (EFL). This quantity, EFL, in Eq. 4.3 is the constant-amplitude stress that causes an equivalent amount of damage over the same number of cycles as that of the observed variable-amplitude stress time series.

$$EFL = \sqrt[m]{\sum_{i=1}^{N} \frac{S_i^m}{N}} \tag{4.3}$$

Then, Eq. 4.2 can be rewritten as follows:

$$D = \frac{N(EFL^m)}{K} \tag{4.4}$$

The following section deals with turbine blade and tower loads based on these equivalent fatigue loads. Fatigue damage histograms computed using the rainflow cycle-counting algorithm are also demonstrated.

4.3.2 Fatigue histograms and equivalent fatigue loads

To estimate equivalent fatigue load for wind turbine loads, a Wohler exponent of $m = 3$ is applied for the steel tower and $m = 10$ is used for the blades composed of fiber composite material.

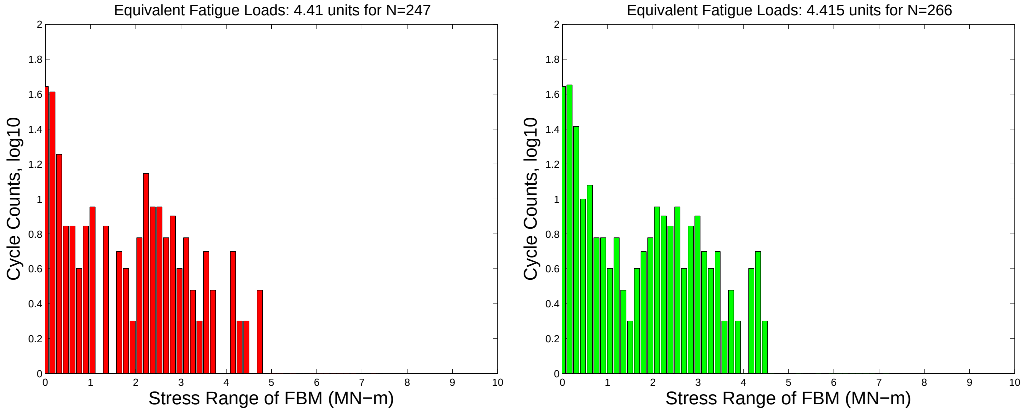

(a) LES (b) LES + FIT

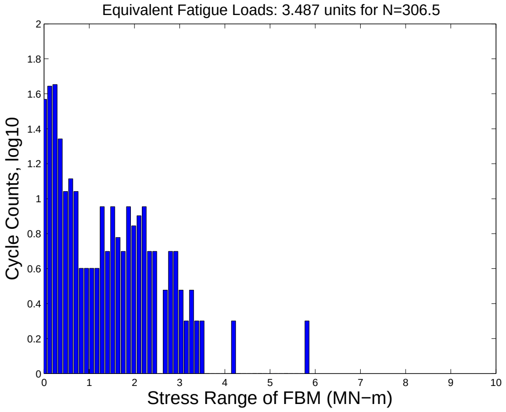

(c) TurbSim

Figure 4.16: Fatigue stress range histograms of FBM.

From each of the 15 simulated time series available, stress range cycles were counted using the rainflow cycle counting algorithm. The counted stress cycles were translated into histograms and the equivalent fatigue load was also computed. Figures 4.16 and 4.17 show fatigue stress range histograms of FBM and TBM, respectively.

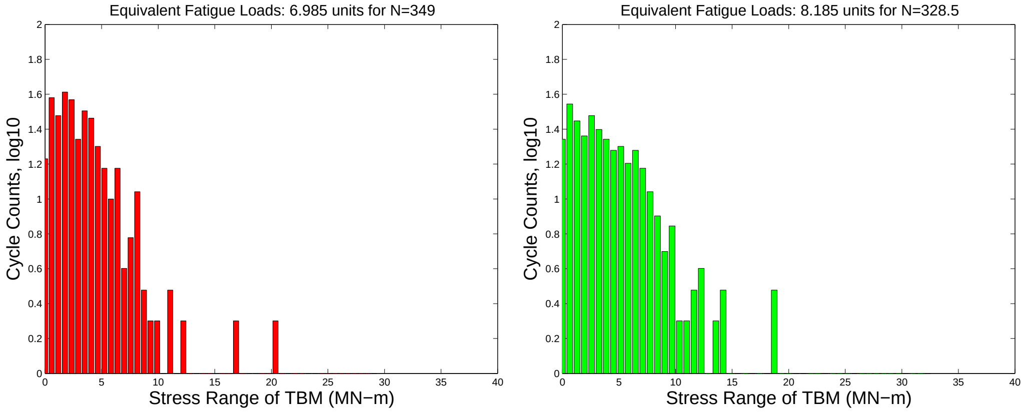

(a) LES (b) LES + FIT

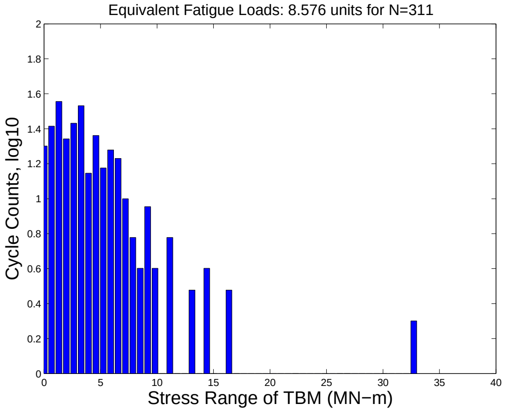

(c) TurbSim

Figure 4.17: Fatigue stress range histograms of TBM.

Stress range histograms based on LES flows are lacking some of the stress cycles compared to the those from the TurbSim flows. It is evident that fractal interpolation helps by filling in some of the missing cycles. Fatigue damage on the blades is somewhat larger for the LES inflow than for the TurbSim inflow. Fractal interpolation, with the additional high-frequency energy, increases the fatigue damage even more relative to the TurbSim inflow. However, for tower loads, the equivalent fatigue load for LES inflow had about a 25% difference with the loads derived from TurbSim inflow before FIT was applied. After fractal interpolation, the equivalent fatigue load became comparable with that from TurbSim inflow.

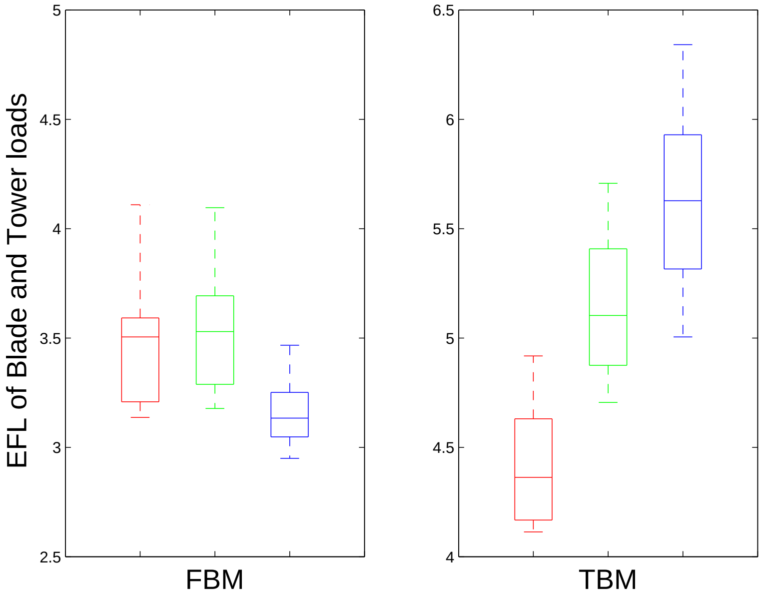

Figure 4.18: Box plot of equivalent fatigue load for blade and tower loads

Figure 4.18 shows box plots of the equivalent fatigue loads for FBM and TBM from 15 simulations. The red box, green box, and blue box represent the LES, LES with FIT, and TurbSim cases, respectively. The equivalent fatigue load (EFL) for blade loads are at comparable levels for LES and TurbSim inflow and fractal interpolation of LES does not change the EFL estimate greatly. However, as was seen with the stress range histograms, the EFL for tower loads improves considerably and becomes comparable to that from TurbSim inflow when fractal interpolation is introduced to the LES inflow turbulence.

Table 4.3: Ensemble estimates of equivalent fatigue load.

Wind Speed	Simulation Type	Equivalent Fatigue Load			
		FBM	EBM	TBM	TTD
12 m/s	LES	3.503	6.017	4.391	0.019
	LES+FIT	3.532	6.015	5.127	0.022
	TurbSim	3.160	5.919	5.644	0.025
15 m/s	LES	4.528	5.842	5.851	0.025
	LES+FIT	4.556	5.854	6.818	0.029
	TurbSim	4.136	5.851	7.111	0.031
17 m/s	LES	5.052	5.782	6.813	0.029
	LES+FIT	4.993	5.809	7.876	0.033
	TurbSim	4.823	5.844	8.459	0.036

Table 4.3 show ensemble statistics of EFL for various loads. EFL estimates for blade loads from LES and TurbSim are comparable even before fractal interpolation is applied. On the other hand, EFL estimates for tower loads improve so as to match very well with TurbSim-generated loads after FIT is applied. This is due to the fractal interpolation that brings high-frequency energy to LES inflow. High-frequency energy is relatively less important in blade loads where the load is controlled by low-frequency energy. For tower loads, where the second mode is at somewhat higher frequencies than the blade loads, the introduction of some high-frequency stress cycles cause an increase

in the equivalent fatigue load of LES inflow to a comparable level with the stochastic inflow.

4.4 Long-term Load Estimation

4.4.1 Design for long-term load estimation

The International Electrotechnical Commission (IEC) standard for the design of wind turbines requires practitioners to consider a characteristic load case that requires estimation of a 50-year return period load. In order to estimate this rare load from a limited number of simulations, one should use statistical extrapolation to predict the long-term loads as described in the IEC Guidelines [11]. Design Load Case (DLC) 1.1 in the IEC standard requires inflow turbulence under near-neutral atmospheric conditions and with specified turbulence intensity that should be simulated with a normal turbulence model (NTM). The ten-min average wind speed is treated as a single random variable representing the environment. In addition, to obtain loads for addressing DLC 1.1, the IEC standard requires one to perform aeroelastic simulations for the entire power-producing wind speed range. In this research study, our simulations are limited to three specific wind speeds since the objective of this study was only to evaluate various inflow simulation methods. As a result, we only compute load distributions based on the wind speeds studied; we do not attempt a full long-term load extrapolation.

In order to estimate short-term load extremes from ten-minute time series, one can use either the peak-over-threshold (POT) method or one can extract global or block maxima values. Agarwal [1] demonstrated that the three extreme models, peak-over-threshold(POT), global maxima, and block maxima can all give close long-term predictions if a sufficient number of simulations are available to obtain the distribution tails. Our research was performed based on a limited number of 15 simulations. In order to estimate load distributions form this limited number of simulations, we used block maxima based on one-minute blocks. We assumed that maximum loads in these one-minute blocks are independent of each other. Hence, the short-term global ten-minute maximum (L) distribution can be obtained for any wind speed V_k from the short-term block maxima (L_{block}). In terms of probability of exceedance of any load level, l, the short-term global maxima distribution is as follows:

$$P(L > l|\, V_k) = 1 - [1 - P(L_{block} > l|\, V_k)]^n \tag{4.5}$$

If various wind speed bins are used, the long-term distribution on L can be obtained in terms of the continuous random variable V as follows:

$$P(L > l) = \int_{V_{in}}^{V_{out}} P(L > l\,|V = v) f_v(v) dv \tag{4.6}$$

where $f_v(v)$ is the wind speed probability density function which is taken to be Rayleigh density function.

4.4.2 Block maxima load extremes for statistical extrapolation

We discuss statistical extrapolation of loads generated from LES, LES with FIT, and TurbSim. Instead of using a single maximum value from each simulated ten-minute time series, extremes are extracted from each one-minute block out of the entire time series in order to estimate short-term load distributions. Such short-term distributions can be employed applied in estimation of long-term load distributions if more simulations and other wind speeds are studied.

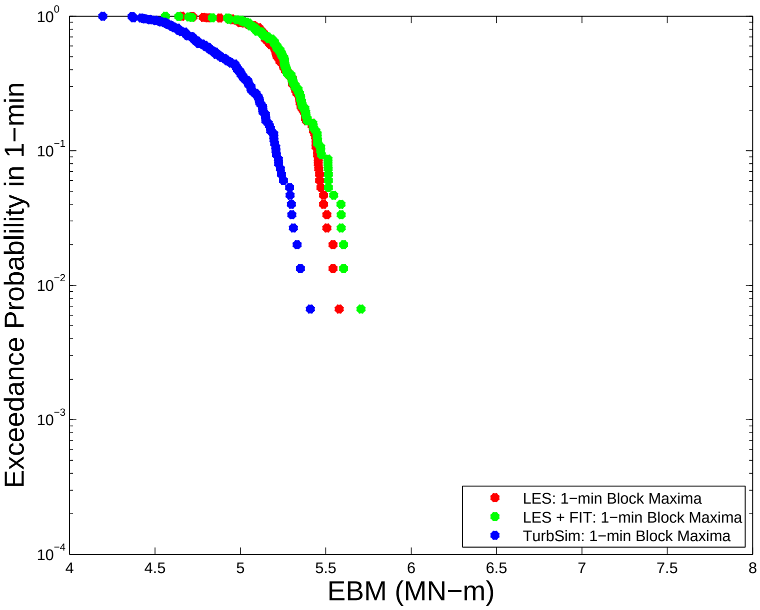

Figure 4.19: Short-term distribution of EBM using 1-min block maxima (mean wind speed = 12 m/s).

First, the time series were split into non-overlapping blocks of constant duration, one-minute. Next, a single largest value is extracted from each time block. These extremes constitute a set of block maxima. The block maxima set are sorted in descending order. Finally, short-term load distributions can be estimated.

Figure 4.19 shows the short-term distribution of EBM loads obtained from inflow turbulence generated by LES, LES with fractal interpolation, and TurbSim for a hub-height mean wind speed of 12 m/s. Fractal interpolation does not change the EBM distribution obtained from LES significantly but it does so at the tail. Although, the loads obtained from LES vary with those from TurbSim, the difference in the 80th percentile ten-minute maximum (or 0.022 non-exceedance probability in 1 min) shows less than 10% difference.

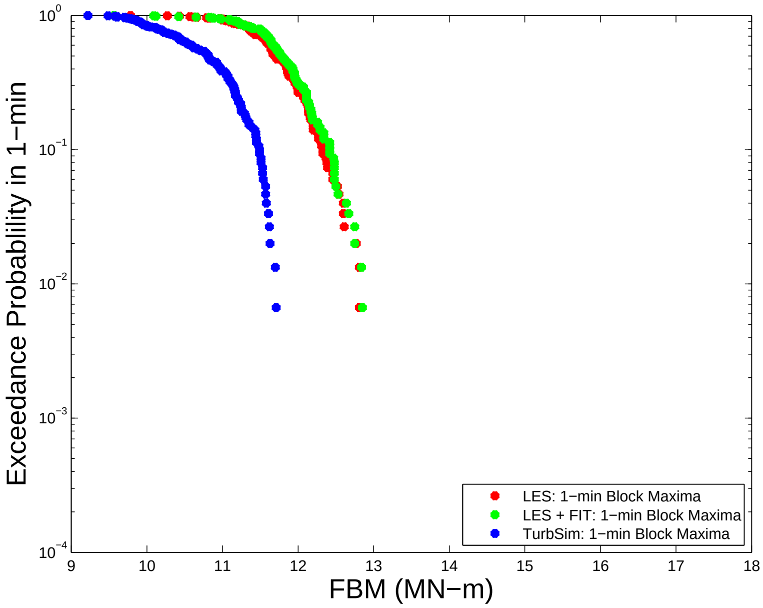

Figure 4.20: Short-term distribution of FBM using 1-min block maxima (mean wind speed = 12 m/s).

Figure 4.20 shows the short-term distribution of FBM loads. For flapwise bending, fractal interpolation leads to no change in load distribution. The difference between LES and TurbSim for the 80th percentile ten-min maximum value is approximately 10% for this load.

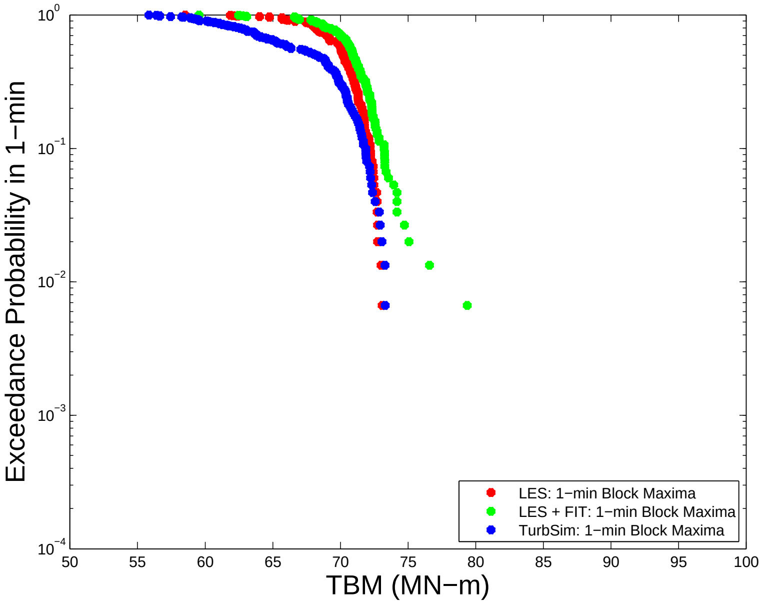

Figure 4.21: Short-term distribution of TBM using 1-min block maxima (mean wind speed = 12 m/s).

Short-term load distributions for the TBM are shown in Fig 4.21. The LES distribution matches that from TurbSim while fractal interpolation introduces a deviation in the tail. Figure 4.22 shows a TBM time series under inflow turbulence generated by LES, LES with FIT, and TurbSim where the largest loads from LES with FIT occurred. It appears that excessive high-frequency energy (around 500 seconds into the record) might have caused some of the large loads that affected the distribution tails. In terms of one-minute (60-second) time blocks, load maxima that are higher than the LES or TurbSim simulation results are also seen in the green time series (FIT). These peaks bring about a deviation on the tail of the short-term distribution. However, this deviation is expected to decrease if more simulations are performed.

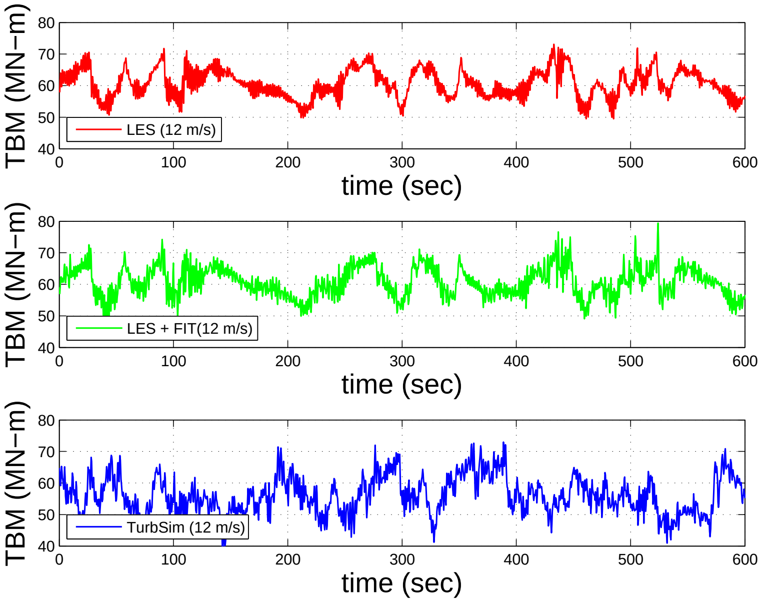

Figure 4.22: Time-histories of TBM under various inflow turbulence

4.5 Summary and Conclusions

Turbine loads under inflow turbulence generated by a different simulation techniques were compared. Inflow turbulence from a neutrally stable boundary layer generated by conventional stochastic simulation, large-eddy simulation, and large-eddy simulation with fractal interpolation was considered. Load statistics were studied to understand the characteristics of turbine loads at different hub-height wind speeds. The hub-height wind speed of 12 m/s had the maximum loads compared to the wind speeds of 15 m/s or 17 m/s. In addition, the dynamic characteristic of turbine loads were studied using power spectral densities of those loads. PSDs of turbine tower loads demonstrated that fractal interpolation can be a promising technique to fill in the energy loss at high frequencies in large-eddy simulations. Next, equivalent fatigue loads and fatigue stress range histograms were studied. Fatigue load studies show that fractal interpolation can improve the stress cycle histograms that are deficient for LES cases versus stochastic simulation cases. Finally, short-term load distributions of turbine loads were studied for possible future long-term load estimations. Due to the limited number of simulations, short-term load distributions were computed based on block maxima of loads; these distributions were reasonably consistent with each other for the LES, LES with FIT, and TurbSim flows. Based on the various turbine load studies conducted here, it is concluded that large-eddy simulations with fractal interpolation can generate turbine loads that are comparable with the stochastic simulation results. For fatigue and ultimate limit states, LES with FIT might be an attractive alternative to stochastic simulation. Having demonstrated its effectiveness as have done here, LES with FIT can now be employed to assess loads on turbines in complex stable boundary layers.

Chapter 5

Conclusions

5.1 Overview of this Research Study

This research study focused on the application of large-eddy simulation (LES) for generating inflow turbulence for wind turbine load studies. In particular, inflow turbulence for neutrally stable boundary layer was studied. This allowed direct comparison with turbine loads produced under inflow turbulence that was generated using conventional stochastic simulation that can be carried out by programs such as NREL's TurbSim.

Since LES required a large amount of computational effort compared to stochastic simulations, the adequate temporal and spatial sampling to generate full-field inflow turbulence was studied prior to any LES-based analyses. This part of the study was based on stochastic simulations where we employed various spectral filters and different grid spacings and compared loads.

After determining the minimal required temporal and spatial sampling to generate inflow turbulence for accurate loads, large-eddy simulations (LES) were run and the full-field inflow turbulence was compared with that generated by stochastic simulations. Due to the lack of high-frequency energy in LES turbulence, a fractal interpolation technique (FIT) was introduced to improve the energy content in LES especially at high frequencies.

Finally, turbine loads generated by LES, LES with FIT, and TurbSim were compared. Various statistics of turbine loads were studied first. Next, power spectral densities, stress range histograms, equivalent fatigue loads, and short-term distribution of turbine load extremes were studied.

The key focus of this thesis was to demonstrate whether turbine loads generated by large-eddy simulation are comparable with loads produced by conventional Fourier techniques. On the basis of the comparisons made, it is believed that LES with FIT can indeed be used for turbine loads analyses. More importantly, LES will be important for addressing wind turbine design issues for nocturnal stable boundary layer (SBL) flows. Since stochastic simulation has limitations in modeling the complex behavior of stable boundary layer flow, LES will make it possible to generate inflow turbulence that can be used for future wind turbine blade and tower design for such SBL flows. This research has led to several specific conclusions that are presented next.

5.2 Conclusions

5.2.1 Temporal and Spatial Sampling of Inflow Turbulence

The computational effort required in LES is dependent on the temporal and spatial sampling rates for inflow turbulence specification. Since our overall goal is to use LES in generating inflow turbulence for wind turbine load studies, a study of the adequate or minimal required temporal and spatial sampling of inflow turbulence was undertaken. Spectral cut-off filters were applied to the full-field inflow generated by stochastic simulations. Although the energy in low-pass filtered winds drops considerably as greater amounts of filtering are applied to the inflow, the load characteristics do not change significantly due to filtering. Filtering out all the energy above 1 Hz from the inflow turbulence still retains important peaks in the load power spectral densities. A time step of 1 Hz and a grid spacing of around one-tenth of the rotor diameter (10 m) could serve as an adequate temporal and spatial resolution of inflow turbulence field in order to estimate turbine loads with less than 5% error for the 5MW utility-scale wind turbine studied.

5.2.2 Atmospheric and Stochastic Simulation of Inflow Turbulence

Large-eddy simulation (LES), which is widely used in the atmospheric sciences, has not been used very much in wind turbine load studies. LES can preserve most of the boundary layer characteristics by solving the nonlinear Navier-Stokes equation and satisfying conservation of mass. However, due to the domain size that LES requires, coarse time steps and grid spacings are used to minimize the computational effort required in such simulations.

LES also gives inflow turbulence that lacks high-frequency energy (small fluctuations in turbulence) compared to the inflow generated by TurbSim. For such reasons, a technique referred to as fractal interpolation was applied to the inflow produced from LES. This fractal interpolation technique (FIT) is an iterative affine mapping procedure that allows one to construct synthetic deterministic small-scale fluctuations from a few given large-scale interpolating points. FIT is an inexpensive computational method that can also preserve higher-order moments and the non-Gaussian probability density of the velocity increments.

It was shown that such FIT enhancements to LES inflow turbulence can enhance the portion of deficient high-frequency energy significantly so that such "LES with FIT" flows have a comparable level of inflow turbulence that that generated by stochastic simulation. This was demonstrated for a neutrally stable boundary layer.

5.2.3 Estimation of Extreme and Fatigue Turbine Loads

Turbine blade and tower loads on a 5MW turbine model produced from aeroelastic simulations with inflow turbulence generated by different simulation techniques were studied. Inflow turbulence for a neutrally stable boundary layer was generated by Large-Eddy simulations (LES), Large-Eddy simulation with fractal interpolation technique (FIT), and conventional stochastic simulation (using TurbSim).

Turbine ten-minute extreme and mean load estimates showed that inflow turbulence with hub-height wind speeds of 12 m/s produced the largest loads. Power spectral densities and fatigue stress range histograms showed that LES turbulence together with the application of FIT leads to comparable loads with those from inflow generated using TurbSim.

Short-term load distributions based on LES were generally only slightly different from those based on stochastic simulation. FIT helped reduce the differences in blade short-term load distributions but also caused greater deviation in tower loads due to high-frequency spikes in the load time series that were introduced.

5.3 Concluding Comments and Suggestions for Future Research

In summary, the inflow turbulence obtained from large-eddy simulation (LES) combined with a fractal interpolation technique (FIT) yields turbine loads that are comparable with those from stochastic simulations. Since there are limitations in applying conventional Fourier (stochastic) techniques to model stable boundary layer flows while LES has the capability to simulate these, this suggests that LES can be used for wind turbine design that needs to consider loads that might occur in the stable boundary layer.

Some suggestions for future research are summarized below:

1. The results presented in this study are limited to inflow and loads for a 5MW utility-scale wind turbine. These findings might vary for wind turbines of other sizes since the dynamic characteristics may be different. Different controllers and different rotor speeds might alter some of the findings from this study.

2. This study focused only on inflow turbulence in near-neutral conditions. The study of inflow turbulence in a stratified stable boundary layer (SBL) may be of interest especially for Great Plains sites where low-level jets

and high-shear events that accompany SBL flows are common and might lead to large turbine loads or fatigue damage.

3. In order to compare long-term turbine loads for design (such as the 50-year characteristic load) based on large-eddy simulation with those based on stochastic simulation, the present study should be extended to include more hub-height wind speeds as well as additional simulations.

Bibliography

[1] P. Agarwal. *Structural Reliability of Offshore Wind Turbines.* Ph.D. dissertation, University of Texas at Austin, 2008.

[2] American Society for Testing and Materials Standards, Standard Practices for Cycle Counting in Fatigue Analysis, E1049-85, 1985.

[3] W.C. Anderson, S. Basu, and C.W. Letchford. Comparison of Dynamic Subgrid-scale Models for Simulations of Neutrally Buoyant Shear-driven Atmospheric Boundary Layer Flows. *Enviornmental Fluid Mechanics*, 7:195–215, 2007.

[4] S. Basu, E. Foufoula-Georgiou, and F. F. Porté-Agel. Synthetic Turbulence, Fractal Interpolation, and Large-Eddy Simulation. *Physical Review E*, 70:026310, 2004.

[5] S. Basu and F. Porté-Agel. Large-Eddy Simulation of Stably Stratified Atmospheric Boundary Layer Turbulence: a Scale-Dependent Dynamic Modeling Approach. *Journal of the Atmospheric Sciences*, 63:2074–2091, 2006.

[6] S. Basu, J.-F. Vinuesa, and A. Swift. Dynamic LES Modeling of a Diurnal Cycle. *Journal of Applied Meteorology and Climatology*, 47:1156–1174, 2008.

[7] J. Fogle, P. Agarwal, and L. Manuel. Towards an Improved Understanding of Statistical Extrapolation for Wind Turbine Extreme Loads. *Wind Energy*, 11:613–635, 2008.

[8] M. Germano, U. Piomelli, P. Moin, and W.H. Cabot. A Dynamic Subgrid-scale Eddy Viscosity Model. *Physics of Fluids A*, 3:1760–1765, 1991.

[9] B.J. Geurts. *Elements of Direct and Large-Eddy Simulation.* Edwards, 2003.

[10] M.O.L. Hansen. *Aerodynamics of Wind Turbines.* Earthscan Publications Ltd., 2nd edition, 2008.

[11] International Electronic Commision, Wind Turbines - Part 1: Design Requirements, IEC-61400-1, Edition 3.0, 2007.

[12] J.M. Jonkman and M.L.Jr. Buhl. FAST User's Guide. Technical Report NREL/EL-500-38230, National Renewable Energy Laboratory, Golden, CO, 2005.

[13] J.M. Jonkman and M.L.Jr. Buhl. TurbSim User's Guide. Technical Report NREL/EL-500-41136, National Renewable Energy Laboratory, Golden, CO, 2007.

[14] J.M. Jonkman, S. Butterfield, W. Musial, and G. Scott. Definition of a 5MW Reference Wind Turbine for Offshore System Development. Tech-

nical Report NREL/TP-500-38060, National Renewable Energy Laboratory, Golden, CO, 2007.

[15] N.D. Kelley, B.J. Jonkman, and G.N. Scott. The Great Plains Turbulence Envoironment: Its Orginis,Impact andSimulation. Technical Report NREL/TP-500-40176, National Renewable Energy Laboratory, Golden, CO, 2006.

[16] N.D. Kelley, B.J. Jonkman, G.N. Scott, J.T. Bialasiewicz, and L.S. Redmond. The Impact of Coherent Turbulence on Wind Turbine Aeroelastic Response and Its Simulation. Technical Report NREL/TP-500-38074, National Renewable Energy Laboratory, Golden, CO, 2005.

[17] N.D. Kelley, R.M. Osgood, J.T. Bialasiewicz, and A. Jakubowski. Using Wavelet Analysis to Assess Turbulence/Rotor Interactions. *Wind Energy*, 3:121–134, 2000.

[18] D.K. Lilly. A Proposed Modification of the Germano Subgrid-scale Closure Method. *Physics of Fluids A*, 4:633–635, 1992.

[19] P. Ragan. *Estimation of Long-Term Structural Loads on a Wind Turbine.* M.S. thesis, University of Texas at Austin, 2007.

[20] K. Saranyassontorn and L. Manuel. Low-dimensional Representations of Inflow Turbulence and Wind Turbine Response Using Proper Orthogonal Decomposition. *Journal of Solar Energy Engineering*, 127:553–562, 2005.

[21] J. Smagorinsky. General Circulation Experiments with the Primitive Equations. *Monthly Weather Review*, 91:99–164, 1963.

[22] J.W. Tukey. *Extrapolatory Data Analysis.* New York: Addison-Wesley, 1977.

[23] P.S. Veers. Three-dimensional Wind Simulation. Technical Report SAND88-0152, Sandia National Laboratory, Albuquerque, NM, 1988.

[24] Det Norske Veritas and Risø National Laboratory. *Guidelines for Design of Wind Turbines.* Jydsk Centraltrykkeri, 2nd edition, 2002.

Vita

Chungwook Sim was born in Seoul, Korea on September 2, 1978. He graduated from Jamsil Highschool in 1997. He studied in the School of Civil and Environmental Engineering at Yonsei University where he received the Bachelor of Science degree in 2001. He received Masters of Science degree from the same program in 2003 with a thesis entitled "An Experimental Study on the Fatigue Behavior of Steel-Concrete Composite Bridge Deck". During the following years, he entered the Hyundai Engineering and Construction Co., Ltd. located in Korea. He worked as a research structural engineer at the Hyundai Research Institute of Construction Technology until summer of 2007. He started his new graduate studies at the University of Texas at Austin with the Rotary International Ambassadorial Scholarship in Fall of 2007. He will continue his doctoral studies at Purdue University in West Lafayette, Indiana.

Permanent address: Olympic Village Apt.202-1202
Oryun Dong, Songpa Gu
Seoul, Korea 138-787

This thesis was typeset with LaTeX[†] by the author.

[†] LaTeX is a document preparation system developed by Leslie Lamport as a special version of Donald Knuth's TeX Program.